Cystathionine β-Synthase as a Carbon Monoxide–Sensitive Regulator of Bile Excretion

Tsunehiro Shintani,* Takuya Iwabuchi,* Tomoyoshi Soga, Yuichiro Kato, Takehiro Yamamoto, Naoharu Takano, Takako Hishiki, Yuki Ueno, Satsuki Ikeda, Tadayuki Sakuragawa, Kazuo Ishikawa, Nobuhito Goda, Yuko Kitagawa, Mayumi Kajimura, Kenji Matsumoto, and Makoto Suematsu

Carbon monoxide (CO) is a stress-inducible gas generated by heme oxygenase (HO) eliciting adaptive responses against toxicants; however, mechanisms for its reception remain unknown. Serendipitous observation in metabolome analysis in CO-overproducing livers suggested roles of cystathionine β-synthase (CBS) that rate-limits transsulfuration pathway and H_2S generation, for the gas-responsive receptor. Studies using recombinant CBS indicated that CO binds to the prosthetic heme, stabilizing 6-coordinated CO-Fe(II)-histidine complex to block the activity, whereas nitric oxide (NO) forms 5-coordinated structure without inhibiting it. The CO-overproducing livers down-regulated H_2S to stimulate HCO_3^--dependent choleresis: these responses were attenuated by blocking HO or by donating H_2S. Livers of heterozygous CBS knockout mice neither down-regulated H_2S nor exhibited the choleresis while overproducing CO. In the mouse model of estradiol-induced cholestasis, CO overproduction by inducing HO-1 significantly improved the bile output through stimulating HCO_3^- excretion; such a choleretic response did not occur in the knockout mice. *Conclusion:* Results collected from metabolome analyses suggested that CBS serves as a CO-sensitive modulator of H_2S to support biliary excretion, shedding light on a putative role of the enzyme for stress-elicited adaptive response against bile-dependent detoxification processes. (HEPATOLOGY 2009;49:141-150.)

Carbon monoxide (CO) is generated from inducible heme oxygenase 1 (HO-1) and constitutive heme oxygenase 2 (HO-2), respectively, and has the ability to regulate neurovascular functions,[1,2] apoptotic responses,[3,4] and metabolism of xenobiotics and toxicants.[5,6] This gas is overproduced through increased delivery of heme as a substrate and the HO-1 induction on exposure to stressors such as hypoxia and oxidative stress. Mechanisms by which CO regulates cell functions appear to involve an activation of soluble guanylate cyclase (sGC), the enzyme that allows the gas to bind to the prosthetic heme to synthesize cyclic guanosine monophosphate as a second messenger.[1] Distinct from nitric oxide (NO) that forms 5-coordinated NO-Fe(II) complex to trigger full activation of the enzyme, CO activates this enzyme only modestly because the gas binding stabilizes 6-coordinated CO-Fe(II)-histidine complex.[7] Mitogen-activated protein kinase has also been shown to serve as a CO-responsive signal transducer.[8] Gene disruption of HO-1 increases sensitivity to overproduction of reactive oxygen species, inflammatory mediators or xenobiotic metabolism, whereas the gene transfer or CO inhalation under these circumstances suppresses such pathogenic responses.[7-9] However, direct mechanisms for the CO reception to trigger these adaptive responses of metabolism remain unknown.

Because this gas has the ability to inhibit ferrous form of the prosthetic heme of enzymes, tryptophan 2,3-dioxygenase or cytochromes P450 have been considered puta-

Abbreviations: CBS, cystathionine β-synthase; CE-MS, capillary electrophoresis equipped with mass spectrometry; CO, carbon monoxide; CORM, CO-releasing metal carbonyl tricarbonyldichlororuthenium (II); ES, 17α-ethinylestradiol; GSH, glutathione; GSNO, S-nitrosyl glutathione; H12, liver exposed to 12-hour hemin treatment; NO, nitric oxide; $RuCl_3$, CO-free ruthenium (III) chloride; SAM, S-adenosyl methionine; SE, standard error; sGC, soluble guanylate cyclase.

From the Department of Biochemistry and Integrative Medical Biology, Department of Surgery, School of Medicine, Keio University, Tokyo, Japan; the Institute for Advanced Biosciences, Keio University, Tiuruoka City, Japan; and the First Department of Surgery, College of Medicine, Nagoya University, Nagoya, Japan.

Received July 3, 2008; accepted August 25, 2008.

*These authors contributed equally to this work.

T.H. is a postdoctoral research fellow supported by Grant-in-Aid for Creative Scientific Research 17GS0419 from JSPS in Japan. Development of the methodology for differential metabolomic analyses using contrast-enhanced time of flight/mass spectrometry was supported by Leading Project for Biosimulation from MEXT. T.I. and T.Y. are research associates of Global COE Program for Metabolomic Systems Biology from MEXT and MHLW.

Address reprint requests to: Makoto Suematsu, M.D., Ph.D., Professor and Chair, Department of Biochemistry and Integrative Medical Biology, School of Medicine, Keio University, 35 Shinanomachi, Shinjuku-ku, Tokyo 160-8582, Japan. E-mail: msuem@sc.itc.keio.ac.jp; fax: (81)-3-5363-3466.

Published online in Wiley InterScience (www.interscience.wiley.com).

DOI 10.1002/hep.22604

Potential conflict of interest: Nothing to report.

tive CO-sensitive signal transducers regulating cell functions, including cell proliferation,[10] immune responses,[11] microvascular tone, xenobiotic detoxification, and biliary excretion in the liver.[5,6,12] However, ferrous heme of these enzymes is not only sensitive to CO but to NO. In this context, whether mechanisms by which CO regulates cell and organ functions is not shared by those for NO has not fully been studied yet.

This study aimed to mine novel CO-responsive regulators for stress-inducible adaptation of metabolism. To this end, we have used metabolome analyses based on capillary electrophoresis equipped with mass spectrometry (CE-MS) for systematic mining CO-responsive gaseous signal transducers. The current results suggest that cystathionine β-synthase (CBS), the enzyme rate-limiting transsulfuration pathway is such a novel CO-sensitive regulator of metabolism that plays an important role for quality control of bile excretion under disease conditions.

Materials and Methods

Preparation of Mice. The experimental protocols herein described were approved by our institutional guidelines provided by the Animal Care Committee of Keio University School of Medicine. Mice heterozygous for disruption in the CBS gene were purchased from Jackson Labs (Bar Harbor, MI) and bred at our institution. Male heterozygous CBS-deficient mice ($CBS^{+/-}$) and their littermates ($CBS^{+/+}$), and wild-type B6J mice, which were purchased from Clea Japan, Inc (Kawasaki City, Japan), were used at 8 to 12 weeks of age. Mice were allowed free access to laboratory chow and tap water, and were fasted for 18 hours before experiments. Mice were anesthetized with an intraperitoneal injection of ketamine at 120 mg/kg, and xylidine at 6 mg/kg. Their common bile ducts were ligated in proximity to the duodenum, and the gallbladder was nicked and cannulated with a polyethylene P-10 tube to collect bile for 20 minutes after a 10-minute stabilization period.[6,13] Biliary constituents such as total bile salts, bilirubin-IXα, pH values, and bicarbonate (HCO_3^-) were measured according to previous methods described elsewhere.[13] When necessary, biliary samples were collected into tubes containing 10% trichloroacetate to measure glutathione through high-performance liquid chromatography.[14] Determination of bilirubin-IXα in bile serves as an indicator of HO-mediated heme degradation in the liver that occurs in parallel with endogenous CO generation. Hepatic CO contents were also measured by gas chromatography as described previously,[15] except that the flame ionization detector equipped with a methanizer was used in this study instead of a reduction gas detector. Combination of these methods to determine CO allowed us to distinguish endogenous CO generation from the same gas exogenously administered as an intervention as described in the following session.

Administration of Reagents Studied. Protoheme IX (hemin) was administered at 40 μmol/kg intraperitoneally at 12 hours before surgical preparation for bile collection. This protocol was denoted as liver exposed to 12-hour hemin treatment (H12) treatment in the text. After collecting bile, livers were excised immediately to be snap-frozen in cold methanol, and the lysates served as samples for contrast-enhanced time of flight/mass spectrometry analyses as described later. In separate sets of experiments, liver samples were minced with 10% trichloroacetic acid at 4°C to measure cysteine and glutathione (GSH) through high-performance liquid chromatography to confirm the data collected from contrast-enhanced time of flight/mass spectrometry, when necessary.

A series of protocols were employed to examine roles of HO-derived CO in regulation of H_2S-modulated choleresis in the H12-treated mice. First, zinc protoporphyrin, a potent HO inhibitor, was administered intravenously at 12.5 μmol/hour/kg at 30 minutes before the bile collection; this dose was sufficient to block endogenous CO in the liver. When necessary, tricarbonyldichlororuthenium (II) dimer, the CO-releasing metal carbonyl [tricarbonyldichlororuthenium (II): CORM, Sigma-Aldorich][16] was administered intraportally at 30 minutes before the start of bile collection. When necessary, CO-free ruthenium (III) chloride ($RuCl_3$) was used as a negative control reagent. To examine whether the elevation of H_2S in the liver could alter biliary HCO_3^- excretion, sodium hydrosulfide (NaHS) was administered at 20 μmol/hour/kg through the portal vein at 30 minutes before the bile collection; as seen later in Results, this protocol restored the H12-induced decrease in the hepatic H_2S contents without altering a reduction of systemic blood pressure that was induced by a systemic bolus of the NaHS injection. S-nitrosyl glutathione (GSNO) was used as an NO donor. The reagent was injected intraportally with a dose of 7 μmol/kg at 30 minutes before the collection of bile; this protocol did not induce a reduction of systemic blood pressure, whereas greater doses caused hypotension and subsequent decrease in the bile output. In these experiments, administration of the reagent was performed through a 30-gauge miniature needle that was inserted into the portal vein to be fixed at the site of puncture. Finally, to examine therapeutic effects of CO, we examined effects of H12 treatment or administration of CORM in the mice exposed to drug-induced cholestasis. To this end, cholestasis was induced by a subcutane-

ous injection of 17α-ethinylestradiol (ES) at 5 mg/kg daily for 5 consecutive days before the experiments.[17]

Metabolome Analysis. We performed metabolome analyses of tissue lysates collected from snap-frozen livers of mice using contrast-enhanced time of flight/mass spectrometry according to our previous methods.[18,19] Measurements of hepatic H_2S contents were based on gas chromatography described in our previous method.[14] Biliary flux of bilirubin-IXα (BR-IXα) in bile samples were determined by enzyme-linked immunosorbent assay using the anti–BR-IXα monoclonal antibody as described previously.[6,20] Because BR-IXα is an end product of the HO-mediated degradation of protoheme IX, its measurements in bile serves as an index of endogenous CO generation in the liver.[20] The conversion of ^{15}N-methionine to its downstream metabolites was determined by CE-MS to examine different rates of the metabolic flux through CBS in the liver. In these experiments, ^{15}N-methionine was intraperitoneally injected at 150 μmol/100 g body weight, and ^{15}N-homocysteine and ^{15}N-cystathionine were measured by CE-MS using the lysates of liver tissues at 30, 60, and 120 minutes after the methionine challenge. Data were expressed as percentages of the mass-labeled metabolites versus total amounts of metabolites in remethylation cycle [ΣRM: methionine + S-adenosyl methionine (SAM) + S-adenosyl homocysteine (SAH) + homocysteine]. In a separate set of experiments, effects of application of CO on contents of methionine and cystathionine in HepG2 cells were determined in culture. In these experiments, the cells were maintained in Roswell Park Memorial Institute 1640 medium (Invitrogen, Carlsbad, CA) containing 10% fetal bovine serum; the mixture was supplemented with 1× penicillin/streptomycin and maintained at 37°C in an atmosphere of 5% CO_2/95% air. The cells were treated with either 50 μmol/L CORM or $RuCl_3$ as a negative control for 16 hours. To measure the metabolites, a frozen pellet of the 1×10^6 cells was homogenized in 10% trichloroacetic acid with 10 mM diethylene triamine pentaacetic acid following brief centrifugation, and the supernatant was used as a sample.

Western Blot Analysis. Western blot analysis was carried out to examine an induction of heme oxygenase (HO)-1 using the polyclonal antibody SPA896 (Stressgen, Ann Arbor, MI). In these experiments, the blotting against α-tubulin was carried out using the polyclonal antibody (Cell Signaling, Danvers, MA) as an internal control.

Recombinant Full-Length Rat CBS. The complementary DNA of the full-length rat CBS was a gift from Professor Masao Ikeda-Saito in Tohoku University. Stopped-flow equipment was purchased from Unisoku, Inc. (Tokyo) and used to examine binding of CO or NO to the CBS protein according to previous methods.[21] Electron paramagnetic resonance spectrometry to determine 5-coordinated structure of the nitrosylheme complex of CBS was carried out according to previous methods.[21,22]

Statistical Analyses. The statistical significance of data among different experimental groups was determined by one-way analysis of variance and Fischer's multiple comparison test. $P < 0.05$ was considered significant.

Results

CO Overproduction Inhibits Transsulfuration and H_2S and Stimulates HCO_3^- Choleresis. Metabolome analyses based on CE-MS allowed us to pinpoint metabolic pathways responding to disease conditions. In mouse liver, we detected more than 1800 metabolites, and compared differences between the control and acetaminophen-treated livers.[18] This method was used to determine differences in metabolic responses between mouse livers and those overloaded with heme, the stressor inducing oxidative stress and subsequent CO overproduction through increasing the substrate and inducing HO-1 (Fig. 1A). The hepatic CO flux peaked at 6 hours, becoming threefold to fourfold greater during the 6 to 12 hours after challenging with hemin, as judged by BR-IXα, an end product of HO-mediated heme degradation (Fig. 1B).[13] Under these conditions, bile output was modestly but significantly increased at 12 to 18 hours after the treatment (Fig. 1C) in parallel with significant elevation of HCO_3^- to make bile more alkaline (Fig. 1D-F), enhancing solubility of organic anions during the detoxification processes. These results suggest that the heme-elicited choleretic response is not correlated with vasodilatory mechanisms by the gas. Based on these results, we used CE-MS analyses to examine metabolomics in the liver exposed to 12-hour hemin treatment (H12), in which phenotypes of bile remodeling became evident.

Among known metabolites (Table 1), most prominent differences between the control and H12 groups occurred in global decreases in amino acids concurrent with increases in Krebs cycle substrates such as acetyl CoA: the fact that these changes coincided with sustained glutamate, significant increases in glutamine, and high-energy adenosine phosphates appeared to suggest utilization of the amino acid pool for energy substrates. By contrast, several essential amino acids such as methionine, tryptophan and histidine, and serine were maintained. Another important alteration was a global decrease in transsulfuration metabolites such as cystathionine, cysteine, and

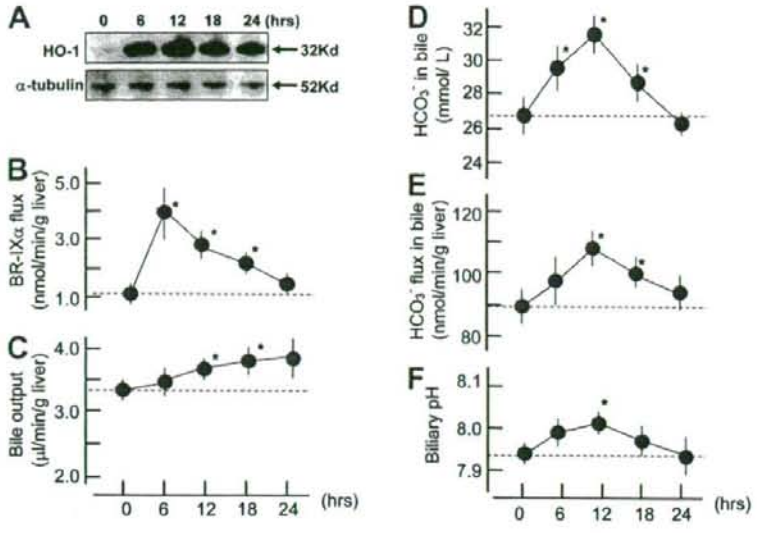

Fig. 1. Temporal alterations in hepatic generation of CO and biliary function after overloading heme. (A) Western blots indicating the induction of heme oxygenase (HO)-1. Alpha-tubulin is an internal control. (B) Biliary excretion of bilirubin-IXα (BR-IXα), a terminal metabolite of HO-dependent heme degradation, as an index of endogenous CO generation through heme oxygenase in the liver. (C) Bile output. (D) Biliary concentration of HCO_3^-. (E) Biliary flux of HCO_3^-. (F) pH values of bile. $^*P < 0.05$ versus the value measured at time 0, which is before the intraperitoneal hemin administration at 40 μmol/kg.

hypotaurine. These results led us to determine tissue contents of H_2S, the terminal product derived from CBS or cystathionine γ-lyase that constitute transsulfuration pathway; this gaseous compound turned out to be suppressed in the H12 group. Based on these measurements, we hypothesized that the H12 treatment limits the activity of CBS so far as judged from maintenance of methionine pool (ΣRM) and serine, a substrate of the enzyme, with suppression of the transsulfuration metabolites residing in the downstream (Fig. 2A). This hypothesis was confirmed by in vivo pulse-chase analysis showing accumulation of ^{15}N-homocysteine and suppression of ^{15}N-cystathionine after the ^{15}N-methionine challenge in the H12 group (Fig. 2B).

Such an inhibitory action of the H12 treatment on the transsulfuration pathway was reproducible when HepG2 cells was treated with CO in culture; contents of cystathionine were significantly suppressed by the application of 50 μmol/L CORM (9.3 ± 1.3 versus 15.9 ± 1.4 nmol/g protein for the vehicle treatment with $RuCl_3$. Mean ± standard error (SE) of three separate experiments, $P < 0.03$), whereas methionine exhibited no difference (66.3 ± 3.7 versus 80.3 ± 12.2 nmol/g protein for CORM and $RuCl_3$, respectively. Mean ± SE of three separate experiments), suggesting inhibitory action of the gas on CBS.

CO But Not NO Inhibits CBS. H12-induced metabolomic changes indicating dissociation between remethylation cycle and transsulfuration pathway led us to hypothesize that CBS, a heme-containing enzyme that rate-limits the transsulfuration pathway, is a sensor of the H12-elicited CO overproduction. Rat full-length recombinant CBS were purified (Fig. 3A) to examine whether CO or NO could inhibit the enzyme activities. CO, but not NO, specifically inhibited the enzyme (Fig. 3B). Previous crystallographic studies using a truncated form of CBS showed that the axial ligands for the prosthetic heme were cysteine and histidine, indicating a large peak of absorbance at 448 nm.[23] On CO application, the heme formed a 6-coordinated CO-Fe(II)–histidine complex, as judged by a decrease in the absorbance at 448 nm and a reciprocal elevation at 422 nm (Fig. 3C). These results were consistent with previous works using the truncated form of human recombinant CBS.[24] Such an inhibitory effect of CO on CBS activity occurred even when sufficient amounts of SAM were present as an allosteric activator,[25] whereas the CO concentrations necessary to suppress CBS became greater in the presence of SAM (Fig. 3D). Conversely, NO was able to bind to the heme but with a distinct structure of 5-coordinated nitrosyl-heme as judged by electron paramagnetic resonance spectrometry (Fig. 3E), suggesting that the enzyme responds specifically to the binding of CO but not that of NO.

CO-Induced HCO_3^- Choleresis Is Sensitive to H_2S and Disappears in CBS$^{+/-}$ Mice. Recent studies indicated that H_2S derived from cystathionine γ-lyase, an enzyme using cysteine to generate the gas, modulates biliary HCO_3^- excretion via mechanisms involving glibenclamide-sensitive channels, a putative H_2S target.[14,26] We hypothesized that the stress-induced CO stimulates the HCO_3^- excretion to increase pH in bile through its inhibitory action on CBS-derived H_2S. To examine this hypothesis, we chose the dose of the CO-releasing molecule (CORM) that was able to increase hepatic contents

Table 1. Comparison of Metabolome Analysis by CE-MS in Liver Extracts Between Control and the Hemin-Treated (H12) Mice

	Control	H12
Carbohydrates (nmol/g liver)		
Glucose 1-P	20 ± 4	31 ± 5
Glucose 6-P	24 ± 1	22 ± 6
Ribulose 5-P	206 ± 60	115 ± 17
Fructose 6-P	25 ± 1	21 ± 6
Glycerol 3-P	1800 ± 250	1663 ± 218
Lactate	3490 ± 633	2920 ± 385
Acetyl CoA	3.4 ± 0.5	6.2 ± 1.1*
Malonyl CoA	37 ± 6	83 ± 15*
Citrate	70 ± 13	88 ± 20
Fumarate	120 ± 22	167 ± 52
Malate	343 ± 91	479 ± 90
CoA	132 ± 21	111 ± 20
Nucleotides (nmol/g liver)		
ATP	208 ± 35	480 ± 90*
GTP	33 ± 4	79 ± 14*
ADP	577 ± 104	1060 ± 154*
AMP	1866 ± 277	1863 ± 70
IMP	501 ± 82	660 ± 99
Adenosine	203 ± 18	151 ± 11
Adenine	12 ± 1	12 ± 2
Hypoxanthine	58 ± 8	43 ± 15
	Control	**H12**
Amino acids (μmol/g liver)		
Gly	3.16 ± 0.11	2.20 ± 0.05*
Ala	3.12 ± 0.48	1.47 ± 0.40*
Ser	0.38 ± 0.07	0.31 ± 0.05
Pro	0.37 ± 0.03	0.27 ± 0.04*
Val	0.41 ± 0.01	0.23 ± 0.05*
Thr	0.31 ± 0.03	0.20 ± 0.04*
Lys	0.69 ± 0.13	0.46 ± 0.05*
Cys	0.20 ± 0.04	0.07 ± 0.03*
Leu	0.36 ± 0.02	0.25 ± 0.05†
Asp	0.76 ± 0.13	0.59 ± 0.12†
Glu	2.90 ± 0.16	2.75 ± 0.28
Gln	3.39 ± 0.58	6.48 ± 0.54*
His	0.43 ± 0.05	0.48 ± 0.02
Amino acids and derivatives (nmol/g liver)		
Met	49 ± 5	39 ± 10
GABA	29 ± 2	25 ± 4
Ornithine	420 ± 95	226 ± 22*
Asn	77 ± 7	59 ± 3*
Ile	175 ± 12	94 ± 17*
Arg	8.8 ± 1.2	4.8 ± 0.6*
Citrulline	64 ± 10	35 ± 3*
Trp	34 ± 2	31 ± 3
Tyr	111 ± 15	52 ± 8*
Glu-2 aminobutyrate	6.3 ± 2.3	5.7 ± 1.2
Ophthalmate	67 ± 7	83 ± 6

Data indicate mean ± SE of six separate experiments.

Data of metabolites in remethylation cycle and transsulfuration pathway were indicated in Fig. 2A.

*$P < 0.05$ and †$P < 0.1$ versus controls.

of CO comparably to those measured in the H12 treatment: As seen (Fig. 4A), the intraportal administration of CORM at 20 μmol/kg significantly increased hepatic CO contents comparable to those induced by H12 treatment in the intact mice. This dose of CORM suppressed hepatic H_2S and stimulated biliary HCO_3^- flux. Stimulatory effects of CO administration on biliary HCO_3^- excretion in intact mice were not shared by NO, as judged by observation in the mice administered with GSNO, an NO donor (Fig. 4B): These results were consistent with observation that CBS is sensitive to CO but not to NO in vitro (Fig. 3).

As already seen, H12 treatment increased CO generation (biliary BR-IXα flux), decreased hepatic H_2S contents, and stimulated biliary HCO_3^- flux (Fig. 1). HO blockade by zinc protoporphyrin-IX cancelled these changes elicited by H12 treatment. On the other hand, an administration of NaHS, an H_2S donor, abolished the H12-induced suppression of hepatic H_2S contents, and significantly attenuated the stimulatory response of biliary HCO_3^- flux (Fig. 5A), suggesting that H12-inducible CO stimulates biliary HCO_3^- excretion through modulation of CBS-derived H_2S. As previously reported, homozygous CBS knockout mice died of severe hepatic steatosis, whereas heterozygous knockout ($CBS^{+/-}$) mice survive through compensation without apparent phenotypes.[27] In these mice, indeed, the baseline H_2S content in livers of $CBS^{+/-}$ mice was comparable to that of $CBS^{+/+}$ mice, presumably because of compensation of the gas generation through cystathionine γ-lyase. On H12 treatment, $CBS^{+/-}$ mice exhibited an increase in the hepatic CO generation comparably to $CBS^{+/+}$ mice, but neither decreased H_2S contents nor up-regulated biliary HCO_3^- flux (Fig. 5B), indicating phenotypes distinct from those in $CBS^{+/+}$ littermates.

CO Protects Against Drug-Induced Cholestasis Through Mechanisms Involving CBS. We further attempted to investigate whether the administration of CO could improve biliary dysfunction occurring in disease models. To examine this, the mice were treated with ES, a cholestatic reagent suppressing three major osmolites such as HCO_3^-, glutathione, and bile salts in bile.[17] H12 treatment or the administration of CORM significantly increased bile output concurrently with a recovery of HCO_3^- excretion into bile (Fig. 6A). The anti-cholestatic effects of H12 treatment through stimulation of HCO_3^- excretion disappeared in the $CBS^{+/-}$ mice (Fig. 6B), suggesting again a pivotal role of CBS for triggering the CO-induced choleresis.

Discussion

CO administration or HO-1 induction has been shown to protect against tissue injury and considered a potentially useful therapeutic stratagem.[8,16] Serendipitous observation in the liver indicating effects of overproduced CO on metabolism of sulfur-containing amino

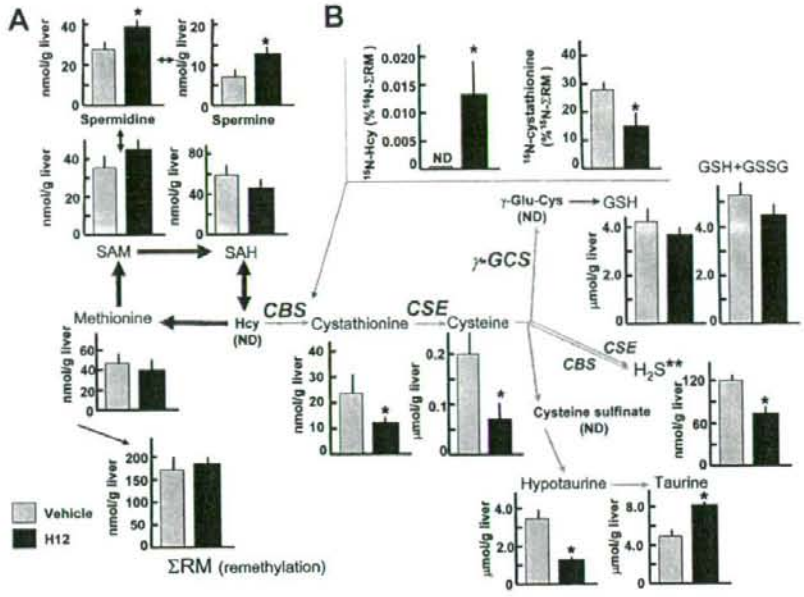

Fig. 2. Metabolomic comparison of sulfur-containing amino acids and their derivatives between the heme-overloaded and vehicle-treated livers of mice. (A) Differences in hepatic contents of the metabolites between the control and hemin-treated mice. H12: treatment with hemin at 12 hours before sampling the liver. Note decreases in transsulfuration metabolites. (B) *In vivo* pulse-chase analysis indicating conversion rates of ^{15}N-methionine into ^{15}N-homocysteine (Hcy) and ^{15}N-cystathionine in livers between the groups. The amounts of the downstream metabolites were measured at 30 minutes after the methionine administration. The data in B were normalized by total amounts of metabolites in remethylation cycle (^{15}N-methionine + ^{15}N-SAM + ^{15}N-SAH + ^{15}N-Hcy = ΣRM) at 30 minutes. ND, not detected. Data indicate mean ± SE of six to eight separate experiments for each group. $^*P < 0.05$ versus the vehicle-treated group.

acids led us to reveal unique physiological actions of this gas on CBS *in vivo* that are not shared with NO. The current study suggested that stress-inducible CO targets CBS and thereby reduces H_2S significantly to stimulate biliary HCO_3^- excretion that could benefit detoxification processes. Conversely, such a property of stress-inducible CO might jeopardize anti-oxidative defense systems through an overflow of homocysteine or through a shortage of GSH. Under current experimental conditions, however, such a risk seemed little, if any, so far as judged from maintenance of GSH and adenosine triphosphate so far. This appears to result from large difference in amino acid pools between methionine (nmol/g) and thiols including cysteine and GSH (μmol/g). Furthermore, cysteine could be supplied through its uptake from extracellular space by mechanisms involving Nrf2, the transcriptional factor activated in response to oxidative stress or electrophiles such as heme.[28,29] By contrast, the amounts of sulfur-containing amino acids consumed to generate H_2S seems relatively smaller than that for synthesizing GSH or hypotaurine, as judged from quantitative information collected by metabolome analysis. Because CBS not only limits synthesis of cystathionine from homocysteine but also directly suppresses H_2S generation from cysteine, the inhibitory effects of CO on the enzyme could dictate largely on the action of H_2S in the liver, causing a stimulatory effect on bile excretion. Considering recent studies suggesting vasodilatory effects of H_2S,[26,30] suppression of CBS-derived H_2S by stress-inducible CO might trigger vasoconstriction, but such vasoactive responses did not occur so far as judged from choleretic response of the basal bile flow that is highly dictated by microvascular perfusion. This might result from the fact that stress-inducible CO itself has the ability to maintain the basal microvascular perfusion through multiple vasodilatory mechanisms involving activation of cyclic guanosine monophosphate and modulation of cytochrome P450–derived vasoconstrictors.[6,20,31]

Although the inhibitory action of stress-inducible CO on the transsulfuration pathway has first been shown in the heme-overloading detoxification model of mice in the current study, a similar event occurred in acetaminophen-induced acute liver injury model of mice in which CO was overproduced through degradation of cytochrome P450–derived heme.[5,18] Our previous study in rats suggested that another HO-derived product bilirubin but not CO

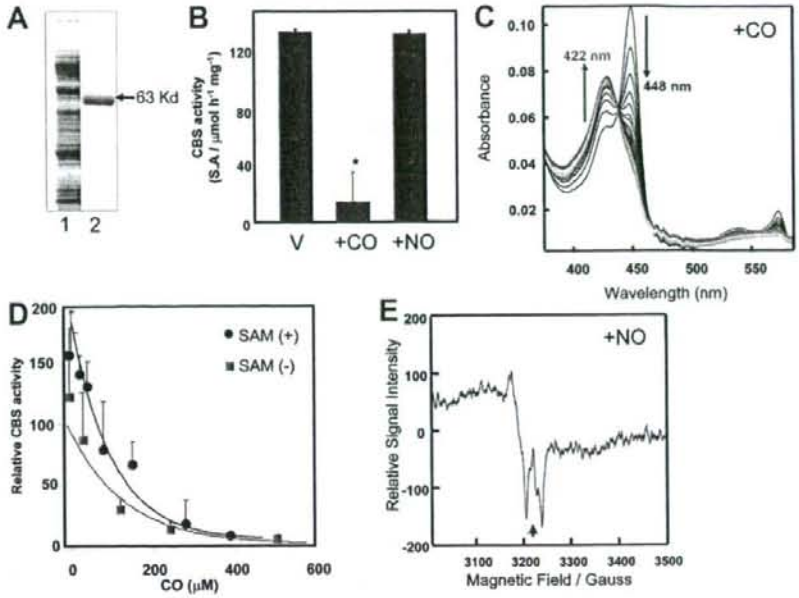

Fig. 3. Effects of CO and NO on the activity and structure of the prosthetic heme of rat recombinant full-length CBS. (A) Sodium dodecyl sulfate polyacrylamide gel electrophoresis for purification of rat recombinant CBS. Lane 1, crude extract; lane 2, purified CBS. (B) Effects of CO and NO on the Fe(II)-CBS activity under optimal substrate conditions at pH 7.4. CO but not NO (100 μM) significantly attenuated the activities of the ferrous enzyme. Data indicate mean ± SE of four experiments. The activities were measured by determining conversion of homocysteine and serine to cystathionine. *$P < 0.05$ versus the group treated with vehicle (V). The concentration of CBS-heme was 10 μM. (C) Stopped-flow visible spectrophotometry for Fe(II)-CBS to examine temporal transitional changes after mixing with CO. Data exhibited a drop at 449 nm and a reciprocal elevation at 422 nm, demonstrating stabilization of the 6-coordinated CO-Fe(II)-histidine complex. K_{obs} = 0.638/second. (D) Effects of CO on the CBS activities in the presence or absence of S-adenosyl methionine (SAM), the allosteric activator of the enzyme. (E) Electron spin resonance spectrometry indicating 5-coordinated NO-Fe(II) complex of the CBS-heme. Arrow: g-value = 2.008.

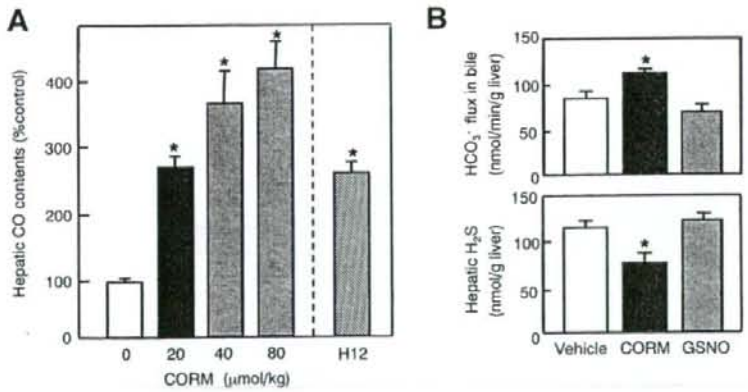

Fig. 4. Effects of the administration of CORM on hepatic CO delivery and biliary function, and their comparison with GSNO, an NO donor. (A) Effects of administration of CORM on hepatic CO contents. H12: the CO contents measured at 12 hours after an intraperitoneal injection of hemin at 40 μmol/kg. Data indicate mean ± SE of five separate experiments for each group. *$P < 0.05$ versus the controls. Note that 20 μmol/kg CORM caused an increase comparable to that induced by H12. (B) Effects of an intraportal administration of CORM on hepatic H_2S contents and biliary HCO_3^- flux. GSNO, S-nitrosyl glutathione, an NO donor. *$P < 0.05$ versus the values in the vehicle-treated controls. Data indicate mean ± SE of seven to eight separate experiments for each group.

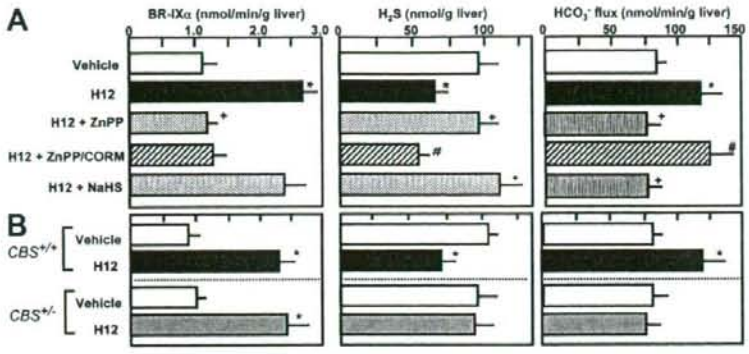

Fig. 5. Effects of HO blockade by zinc protoporphyrin and supplementation of NaHS, an H_2S donor, on biliary flux of BR-IXα, hepatic H_2S contents, and biliary HCO_3^- excretion in the 12-hour hemin-treated liver (H12). (A) Measurements in wild-type male B6 mice. Note that the hemin-induced suppression of H_2S generation and stimulation of biliary HCO_3^- excretion were sensitive to the HO inhibitor and reversed by supplementing CO (CORM). An injection of NaHS, an H_2S donor, restored hepatic H_2S contents and repressed the biliary HCO_3^- excretion in the H12-treated liver, suggesting that the biliary response is H_2S-dependent. (B) Disappearance of H12-induced reduction of H_2S and biliary HCO_3^- excretion in heterozygous CBS-knockout mice ($CBS^{+/-}$). Note that $CBS^{+/-}$ mice neither exhibit a reduction of H_2S nor up-regulate biliary HCO_3^- excretion, although overproducing CO (BR-IXα flux) comparably to the littermates ($CBS^{+/+}$). $^*P < 0.05$ versus the vehicle-treated controls. $^+P < 0.05$ versus the H12-treated groups. $^\#P < 0.05$ versus the H12+ zinc protoporphyrin-treated groups.

has the ability to improve bile acid–dependent bile output of the post–cold ischemic liver grafts through its antioxidative action.[32] However, such an effect of bilirubin appears to be distinct from the stimulatory action of CO on biliary fluid excretion indicated in the current study. CO has been shown to exert diverse actions on biliary function through multiple mechanisms: First, stress-inducible levels of CO have the ability to elongate the intervals of bile canalicular contraction, which helps increase the stroke volume for promoting bile excretion; this process appears to involve mechanisms mediated by modulation of cytochrome P450 epoxygenases and intra-

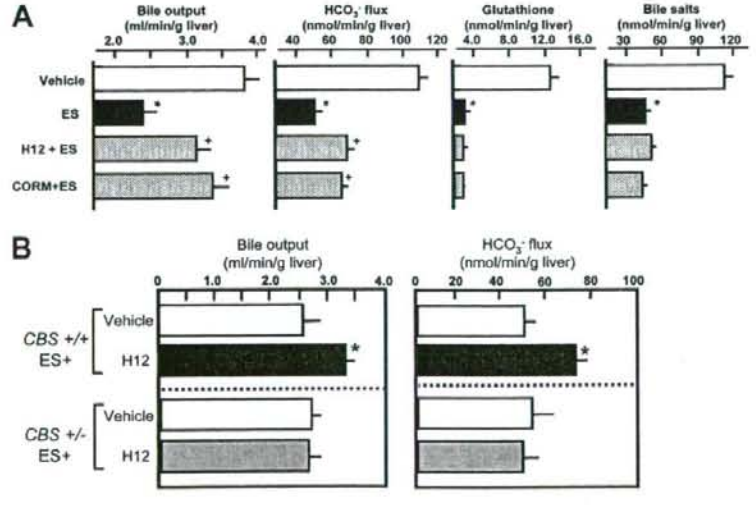

Fig. 6. Effects of H12 treatment or CORM administration on 17α-ethinylestradiol (ES)-induced cholestasis in male B6 mice. (A) Effects of H12 or CORM on ES-induced decreases in the bile output and bile constituents. ES elicited marked cholestasis, which coincided with decreases in HCO_3^-, glutathione, and bile salts in bile. Pretreatment with hemin at 12 hours before the administration of ES (H12 + ES) or the administration of CORM significantly attenuated ES-induced cholestasis through stimulation of HCO_3^- excretion into bile. (B) Effects of H12 treatment on ES-induced impairment of bile output and biliary HCO_3^- flux in $CBS^{+/+}$ and $CBS^{+/-}$ mice. $^*P < 0.05$ versus the values in vehicle-treated controls. $^+P < 0.05$ versus the values in ES-treated group. Data indicate mean ± SE of eight separate experiments for each group. Note disappearance of the improving effect of H12 treatment in the $CBS^{+/-}$ mice.

cellular Ca^{2+} mobilization.[12] Second, suppression of endogenous CO activates bile acid–dependent bile excretion through accelerated vesicular transport of taurocholate, while inducing no significant elevation of the bile acid–independent fraction.[33] Conversely, CO overproduction by the HO-1 induction or exogenous administration of CO stimulates bile acid–independent choleresis concurrently with increased mrp2-dependent excretion of bilirubin-IXα and glutathione, while suppressing biliary excretion of bile salts, indicating the effects of the gas for stimulating fluid excretion into bile.[34] Of interest is that glibenclamide, an inhibitor of K^+ channel that serves as a putative target for H_2S,[26] acts on Na^+-K^+-$2Cl^-$ cotransporter in bile duct epithelium to stimulate biliary HCO_3^- excretion in normal and cholestatic livers.[35] We showed that inhibition of cystathionine γ-lyase, another H_2S-generating enzyme, stimulates basal and glibenclamide-induced fluid output of bile through stimulating HCO_3^- excretion without altering the baseline vascular resistance of the liver.[14] Recent studies provided evidence that such a glibenclamide-responsive channel is present in rodent cholangiocytes[36] or in duodenum,[37] contributing to stimulation of the HCO_3^- excretion.[36] Based on these observations, it is not unreasonable to speculate that CO stimulates biliary fluid excretion through mechanisms involving H_2S-mediated modulation of glibenclamide-sensitive channels on biliary epithelium. Although further investigation is necessary to determine whether these mechanisms are sensitive to H_2S, the current results shed light on a possibility that the CO-CBS system serves as a putative mechanism for stimulating bile acid–independent fluid excretion, facilitating excretion of HCO_3^- and organic anions such as bilirubin to support heme detoxification. Both glibenclamide and CO help biliary fluid excretion in estrogen-induced hepatocellular cholestasis. Exploration of H_2S-sensitive molecular targets occurring on biliary epithelium deserves further studies for evidence that HO-1–derived CO serves as a therapeutic stratagem for protecting against cholestasis.

CO has been believed to share varied physiological effects on biological systems with NO. However, through extrapolation of studies *in vitro* indicating biochemical actions of CO to trigger structural changes in gas-responsive heme proteins (such as sGC, hemoglobin) distinct from those elicited by NO,[7,19,21,22,38] evidence that CO is a unique gaseous regulator distinct from NO has been emerging. In fact, CO itself modestly activates sGC, by which hepatic sinusoids are constitutively dilated.[2,20,39] By contrast, in vascular smooth muscle cells in which NO is sufficiently supplied from arteriolar endothelium (for example, brain microcirculation), the inducible CO inhibits NO-elicited sGC activation.[40,41] Besides these observations suggesting physiologic actions of CO occurring dependently of local NO levels, the current study provided evidence for a novel mechanism functioning irrespective of the NO effects. Furthermore, our results shed light on a metabolic link between CO and H_2S, suggesting that different gaseous mediators constitute an intriguing link for regulation of organ functions.

Acknowledgment: The authors thank Kayo Maruyama for technical support in measuring tissue H_2S contents.

References

1. Verma A, Hirsch DJ, Glatt CE, Ronnett GV, Snyder SH. Carbon monoxide: a putative neural messenger. Science 1993;259:381-384.
2. Suematsu M, Goda N, Sano T, Kashiwagi S, Egawa T, Shinoda Y, et al. Carbon monoxide: an endogenous modulator of sinusoidal tone in the perfused rat liver. J Clin Invest 1995;96:2431-2437.
3. Ozawa N, Goda N, Makino N, Yamaguchi T, Yoshimura Y, Suematsu M. Leydig cell-derived heme oxygenase-1 regulates apoptosis of premeiotic germ cells in response to stress. J Clin Invest 2002;109:457-467.
4. Song R, Zhou Z, Kim PK, Shapiro RA, Liu F, Ferran C, et al. Carbon monoxide promotes Fas/CD95-induced apoptosis in Jurkat cells. J Biol Chem 2004;279:44327-44334.
5. Mori M, Suematsu M, Kyokane T, Sano T, Suzuki H, Yamaguchi T, et al. Carbon monoxide-mediated alterations in paracellular permeability and vesicular transport in acetaminophen-treated perfused rat liver. HEPATOLOGY 1999;30:160-168.
6. Kyokane T, Norimizu S, Taniai H, Yamaguchi T, Takeoka S, Tsuchida E, et al. Carbon monoxide from heme catabolism protects against hepatobiliary dysfunction in endotoxin-treated rat liver. Gastroenterology 2001;120:1227-1240.
7. Zhao Y, Brandish PE, Ballou DP, Marletta MA. A molecular basis for nitric oxide sensing by soluble guanylate cyclase. Proc Natl Acad Sci U S A 1999;96:14753-14758.
8. Otterbein LE, Bach FH, Alam J, Soares M, Tao Lu H, Wysk M, et al. Carbon monoxide has anti-inflammatory effects involving the mitogen-activated protein kinase pathway. Nat Med 2000;6:422-428.
9. Abraham NG, Quan S, Mieyal PA, Yang L, Burke-Wolin T, Mingone CJ, et al. Modulation of cGMP by human HO-1 retrovirus gene transfer in pulmonary microvessel endothelial cells. Am J Physiol Lung Cell Mol Physiol 2002;283:L1117-L1124.
10. Hill M, Pereira V, Chauveau C, Zagani R, Remy S, Tesson L, et al. Heme oxygenase-1 inhibits rat and human breast cancer cell proliferation: mutual cross inhibition with indoleamine 2,3-dioxygenase. FASEB J 2005;19:1957-1968.
11. Thomas SR, Mohr D, Stocker R. Nitric oxide inhibits indoleamine 2,3-dioxygenase activity in interferon-gamma primed mononuclear phagocytes. J Biol Chem 1994;269:14457-14464.
12. Shinoda Y, Suematsu M, Wakabayashi Y, Suzuki T, Goda N, Saito S, et al. Carbon monoxide as a regulator of bile canalicular contractility in cultured rat hepatocytes. HEPATOLOGY 1998;28:286-295.
13. Wakabayashi Y, Takamiya R, Mizuki A, Kyokane T, Goda N, Yamaguchi T, et al. Carbon monoxide overproduced by heme oxygenase-1 causes a reduction of vascular resistance in perfused rat liver. Am J Physiol 1999;277:G1088-G1096.
14. Fujii K, Sakuragawa T, Kashiba M, Sugiura Y, Kondo M, Maruyama K, et al. Hydrogen sulfide as an endogenous modulator of biliary bicarbonate excretion in the rat liver. Antioxid Redox Signal 2005;7:788-794.
15. Vreman HJ, Wong RJ, Kadotani T, Stevenson DK. Determination of carbon monoxide (CO) in rodent tissue: effect of heme administration and environmental CO exposure. Anal Biochem 2005;341:280-289.

16. Motterlini R, Clark JE, Foresti R, Sarathchandra P, Mann BE, Green CJ. Carbon monoxide-releasing molecules: characterization of biochemical and vascular activities. Circ Res 2002;90:e17-e24.
17. Bossard R, Stieger B, O'Neill B, Fricker G, Meier PJ. Ethinylestradiol treatment induces multiple canalicular membrane transport alterations in rat liver. J Clin Invest 1993;91:2714-2720.
18. Soga T, Baran R, Suematsu M, Ueno Y, Ikeda S, Sakurakawa T, et al. Differential metabolomics reveals ophthalmic acid as an oxidative stress biomarker indicating hepatic glutathione consumption. J Biol Chem 2006;281:16768-16776.
19. Kinoshita A, Tsukada K, Soga T, Hishiki T, Ueno Y, Nakayama Y, et al. Roles of hemoglobin allostery in hypoxia-induced metabolic alterations in erythrocytes: simulation and its verification by metabolome analysis. J Biol Chem 2007;282:10731-10741.
20. Goda N, Suzuki K, Naito M, Takeoka S, Tsuchida E, Ishimura Y, et al. Distribution of heme oxygenase isoforms in rat liver: topographic basis for carbon monoxide-mediated microvascular relaxation. J Clin Invest 1998; 101:604-612.
21. Yonetani T, Tsuneshige A, Zhou Y, Chen X. Electron paramagnetic resonance and oxygen binding studies of alpha-nitrosyl hemoglobin: a novel oxygen carrier having NO-assisted allosteric functions. J Biol Chem 1998; 273:20323-20333.
22. Suganuma K, Tsukada K, Kashiba M, Tsuneshige A, Furukawa T, Kubota T, et al. Erythrocytes with T-state-stabilized hemoglobin as a therapeutic tool for postischemic liver dysfunction. Antioxid Redox Signal 2006;8: 1847-1855.
23. Meier M, Janosik M, Kery V, Kraus JP, Burkhard P. Structure of human cystathionine beta-synthase: a unique pyridoxal 5'-phosphate-dependent heme protein. EMBO J 2001;20:3910-3916.
24. Taoka S, Banerjee R. Characterization of NO binding to human cystathionine beta-synthase: possible implications of the effects of CO and NO binding to the human enzyme. J Inorg Biochem 2001;87:245-251.
25. Prudova A, Bauman Z, Braun A, Vitvitsky V, Lu SC, Banerjee R. S-adenosylmethionine stabilizes cystathionine beta-synthase and modulates redox capacity. Proc Natl Acad Sci USA 2006;103:6489-6494.
26. Zhao W, Zhang J, Lu Y, Wang R. The vasorelaxant effect of H_2S as a novel endogenous gaseous K_{ATP} channel opener. EMBO J 2001;20:6008-6016.
27. Werstuck GH, Lentz SR, Dayal S, Hossain GS, Sood SK, Shi YY, et al. Homocysteine-induced endoplasmic reticulum stress causes dysregulation of the cholesterol and triglyceride biosynthetic pathways. J Clin Invest 2001;107:1263-1273.
28. Maher JM, Dieter MZ, Aleksunes LM, Slitt AL, Guo G, Tanaka Y, et al. Oxidative and electrophilic stress induces multidrug resistance-associated protein transporters via the nuclear factor-E2-related factor-2 transcriptional pathway. HEPATOLOGY 2007;46:1597-1610.
29. Sasaki H, Sato H, Kuriyama-Matsumura K, Sato K, Maebara K, Wang H, et al. Electrophile response element-mediated induction of the cystine/glutamate exchange transporter gene expression. J Biol Chem 2002;277: 44765-44771.
30. Fiorucci S, Antonelli E, Mencarelli A, Orlandi S, Renga B, Rizzo G, et al. The third gas: H_2S regulates perfusion pressure in both the isolated and perfused normal rat liver and in cirrhosis. HEPATOLOGY 2005;42:539-548.
31. Suematsu M, Ishimura Y. The heme oxygenase-carbon monoxide system: a regulator of hepatobiliary function. HEPATOLOGY 2000;31:3-6.
32. Kato Y, Shimazu M, Kondo M, Uchida K, Kumamoto Y, Wakabayashi G, et al. Bilirubin rinse: a simple protectant against the rat liver graft injury mimicking heme oxygenase-1 preconditioning. HEPATOLOGY 2003;38:364-373.
33. Sano T, Shiomi M, Wakabayashi Y, Shinoda Y, Goda N, Yamaguchi T, et al. Endogenous carbon monoxide suppression stimulates bile acid-dependent biliary transport in perfused rat liver. Am J Physiol 1997;272:G1268-G1275.
34. Norimizu S, Kudo A, Kajimura M, Ishikawa K, Taniai H, Yamaguchi T, et al. Carbon monoxide stimulates mrp2-dependent excretion of bilirubin-IXα into bile in the perfused rat liver. Antioxid Redox Signal 2003;5:449-456.
35. Nathanson MH, Burgstahler AD, Mennone A, Dranoff JA, Rios-Velez L. Stimulation of bile duct epithelial secretion by glybenclamide in normal and cholestatic rat liver. J Clin Invest 1998;101:2665-2676.
36. Spirli C, Fiorotto R, Song L, Santos-Sacchi J, Okolicsanyi L, Masier S, et al. Glibenclamide stimulates fluid secretion in rodent cholangiocytes through a cystic fibrosis transmembrane conductance regulator-independent mechanism. Gastroenterology 2005;129:220-233.
37. Sellers ZM, Mann E, Smith A, Ko KH, Giannella R, Cohen MB, et al. Heat-stable enterotoxin of Escherichia coli (STa) can stimulate duodenal HCO_3^- secretion via a novel GC-C- and CFTR-independent pathway. FASEB J 2008;22:1306-1316.
38. Boon EM, Huang SH, Marletta MA. A molecular basis for NO selectivity in soluble guanylate cyclase. Nat Chem Biol 2005;1:53-59.
39. Kajimura M, Shimoyama M, Tsuyama S, Suzuki T, Kozaki S, Takenaka S, et al. Visualization of gaseous monoxide reception by soluble guanylate cyclase in the rat retina. FASEB J 2003;17:506-508.
40. Imai T, Morita T, Shindo T, Nagai R, Yazaki Y, Kurihara H, et al. Vascular smooth muscle cell-directed overexpression of heme oxygenase-1 elevates blood pressure through attenuation of nitric oxide-induced vasodilation in mice. Circ Res 2001;89:55-62.
41. Ishikawa M, Kajimura M, Adachi T, Maruyama K, Makino N, Goda N, et al. Carbon monoxide from heme oxygenase-2 is a tonic regulator against NO-dependent vasodilatation in the adult rat cerebral microcirculation. Circ Res 2005;97:e104-e114.

Inhibiting nitric oxide overproduction during hypotensive sepsis increases local oxygen consumption in rat skeletal muscle*

Ryon M. Bateman, PhD; Michael D. Sharpe, MD; Daniel Goldman, PhD; Darcy Lidington, PhD; Christopher G. Ellis, PhD

Objective: Although nitric oxide (NO) is a known regulator of cardiovascular function, the effect of NO overproduction during sepsis on capillary oxygen transport and local tissue oxygen consumption is not well understood. The objectives of this study were to determine whether sepsis-induced NO overproduction increased capillary stopped-flow and modulated tissue oxygen consumption in skeletal muscle.

Design: Prospective, controlled laboratory study.

Setting: Animal laboratory in a university-affiliated research institute.

Subjects: Male Sprague-Dawley rats, 165–180 g body weight.

Interventions: Rats were made septic by cecal ligation and perforation (CLP) and were then ventilated and volume resuscitated (saline). The hind limb extensor digitorum longus (EDL) skeletal muscle was blunt dissected for *in vivo* microvascular imaging. The inducible NO synthase (iNOS) inhibitor L-N6-(1-iminoethyl)lysine dihydrochloride (L-NIL) was infused (3 mg/kg body weight per hour) starting 1 hr post-CLP to maintain arterial blood and EDL tissue NO_x^- (NO_2^- + NO_3^-) at baseline.

Measurements and Main Results: Red blood cell hemodynamics, hemoglobin oxygen saturation, capillary geometry, and functional capillary density information were used to calculate capillary oxygen flux (the rate of oxygen diffusion from capillary to tissue) and indices of local oxygen delivery and tissue oxygen consumption. Over the first 5 hrs of septic injury, mean arterial pressure decreased while capillary stopped-flow and capillary oxygen flux both increased ($p < .05$). Inhibiting iNOS/NO overproduction partially restored mean arterial pressure and increased arterial pH. Within the microcirculation, inhibiting NO increased capillary red cell velocity and increased local tissue oxygen consumption ($p < .05$). Inhibiting NO failed, however, to prevent capillary stopped-flow.

Conclusions: During the onset of sepsis, concurrent with the onset of microvascular dysfunction, there is an iNOS/NO-mediated reduction in local skeletal muscle tissue oxygen consumption. (Crit Care Med 2008; 36:225–231)

KEY WORDS: sepsis; microcirculation; nitric oxide; capillaries; oxygen consumption

Nitric oxide (NO) is a gas produced from L-arginine and oxygen. During sepsis, the overproduction of NO due to up-regulation of inducible NO synthase (iNOS) has been associated with impaired vascular reactivity, capillary leak, decreased erythrocyte deformability, and refractory hypotension (1). *In vitro* experiments have shown that NO inhibits mitochondrial respiration both reversibly and irreversibly, depending on the duration of NO exposure and the mitochondrial complex inhibited (2–5), thereby reducing oxygen consumption. The reversible NO-mediated inhibition of cytochrome *c* oxidase (complex IV) depends on oxygen concentration (5), which *in vivo* would be established by local capillary oxygen delivery and tissue oxygen consumption. Whether iNOS/NO overproduction modulates local *in vivo* tissue oxygen consumption during sepsis is unknown.

Nonspecific NOS inhibition was found to reduce tissue P_{O_2} in skeletal muscle in septic rats (6) and the hind limb of normal dogs (7), whereas more specific iNOS inhibition was found to increase serosal microvascular oxygenation in endotoxemic pigs (8). Initial clinical studies reported that nonspecific NOS inhibition normalized cardiac output and systemic vascular resistance while reducing vasopressor use, without any apparent adverse effects on tissue oxygenation or organ function (9, 10). Seemingly in agreement were the open-label dose escalation study and clinical trial of the nonspecific NOS inhibitor 546C88, which found that while global oxygen extraction increased, oxygen consumption was maintained (11–13). In contrast, Statman et al. (14) reported that nonspecific NOS inhibition increased systemic vascular resistance at the expense of tissue oxygenation in septic patients. While the ultimate failure of the multicenter clinical trial of 546C88 was attributed to cardiovascular death (12), what is not understood in sepsis, in either patients or experimental models, is the overall effect of iNOS/NO overproduction and its inhibition on microvascular oxygen transport and local ox-

*See also p. 359.

From the University of Western Ontario and the London Health Sciences Centre, Department of Medical Biophysics (RMB, DL, CGE) and Department of Anesthesia and Program in Critical Care Medicine (MDS), London, ON, Canada; and the Departments of Mathematical Sciences and Biomedical Engineering, New Jersey Institute of Technology, Newark, NJ (DG).

Supported, in part, by research grant MOP-499416 from the Canadian Institutes of Health, London, ON, Canada, University of Western Ontario (CGE). Dr. Bateman is a Lewis MacDonald Research Fellow and was supported by the Spoerel Research Fellowship (London, ON, Canada) and the Heart and Stroke Foundation of Canada (postdoctoral fellowship). The authors have not disclosed any potential conflicts of interest.

Address requests for reprints to: Ryon M. Bateman, PhD, Department of Biochemistry and Integrative Medical Biology, School of Medicine, Keio University, 35 Shinanomachi, Shinjuku-Ku, Tokyo 160-8582 Japan.

DOI: 10.1097/01.CCM.0000295307.92027.2F

ygen consumption at the most fundamental tissue/capillary level.

To address this issue, we inhibited iNOS/NO overproduction in a rat model of hypotensive sepsis and measured capillary oxygen transport variables. Since nitric oxide synthesis is up-regulated in the first few hours following a septic insult (1), this animal study focuses on whether iNOS/NO overproduction in the early stages of hypotensive sepsis affects capillary flow distribution, capillary hemodynamics, and local tissue oxygen consumption in skeletal muscle. Here we extend our previous work (15–18) by calculating indices for capillary oxygen supply and local tissue oxygen consumption. We hypothesized that complete inhibition of NO overproduction following the onset of a septic insult would 1) prevent the development of capillary stopped-flow and subsequent maldistribution of oxygen delivery that we and others have observed in both early and late stages of sepsis (15, 16, 19); and 2) increase oxygen consumption by preventing NO-induced mitochondrial inhibition. To test these hypotheses, we pharmacologically inhibited NO overproduction in a rat model of hypotensive sepsis and used *in vivo* microvascular imaging to obtain oxygen transport and tissue oxygen consumption data at the capillary level.

MATERIALS AND METHODS

Animals. Nonfasting adult male Sprague-Dawley rats (165–180 g) were randomized to three groups: sham laparotomy (sham, n = 5), cecal ligation and perforation (CLP, n = 5), and CLP treated with the iNOS inhibitor L-N6-(1-iminoethyl)lysine dihydrochloride (CLP+L-NIL, n = 5). Experimental protocols were approved by the University of Western Ontario Council on Animal Care.

Acute CLP Sepsis Model. An acute fecal-peritonitis model of sepsis was used with continuous intravenous infusion of sodium pentobarbital (18 $mg \cdot kg^{-1} \cdot hr^{-1}$) for general anesthesia. The cecum was exposed through a midline incision, ligated distal to the ileocecal valve, and perforated by a 0.5-cm incision. Fecal contents were expressed into the peritoneum and the incision was closed. The right carotid artery and left jugular vein were cannulated (polyethylene-10, Clay Adams, and Bio-Sil tubing, Silmed, Saint-Gobain Akron, OH) for monitoring mean arterial pressure (MAP, Digi-Med Blood Pressure Analyzer, Micro-Med, Louisville, KY) and providing fluid resuscitation (0.9% saline, 10 $mL \cdot kg^{-1} \cdot hr^{-1}$), respectively. Animals were tracheotomized and mechanically ventilated (30%:70% oxygen/nitrogen). Ventilation variables and baseline blood gases were established within the normal range at the outset and were not adjusted during the experiment: Po_2 85–100 torr, Pco_2 35–45 torr, and pH 7.3–7.4 (ABL Radiometer Blood Gas Analyzer, ABL500, Copenhagen, Denmark), respiratory rate 72–85 breaths/min, and tidal volume 1.6–2.2 mL (Harvard Rodent Ventilator, 683, Diversified Equipment, Lorton, VA).

EDL Skeletal Muscle Preparation. Following abdominal surgery, the hind limb extensor digitorum longus (EDL) skeletal muscle was blunt dissected and severed from the tendon. The animal was moved to the imaging stage and the EDL positioned in the optical path at *in situ* length by a suture tied to the tendon. The muscle was covered by Saran-Wrap and cover slip, which acted as an oxygen barrier, and allowed to stabilize for 30 mins. Six to eight random fields of view of microvascular beds were imaged from 3.5 to 4.5 hrs following the septic injury. Equal numbers of random arteriolar-end, mid-vessel, and venular-end capillary segments were recorded for 1–2 mins. Animal core temperature was maintained between 36.5°C and 37.2°C by external heat lamp.

Functional Microvascular Imaging: Capillary Red Blood Cell Hemodynamics, Hemoglobin Oxygen Saturation, and Geometry. The microvascular imaging system has been described previously (16, 20, 21). In brief, optical density (OD) information at 420 and 430 nm from the EDL skeletal muscle microcirculation was acquired on S-VHS video tape via two high-resolution closed-circuit video systems (video monitor, WV-5410, and video cassette recorder, AG-7300, Panasonic, Osaka, Japan). This was achieved by illuminating the EDL with a 100-W xenon light source (Diaphot 300 inverted microscope, Nikon, Yokohama, Japan, and ×20/0.4 Nikon objective) and splitting the transmitted light 70:30 (beam splitter fitted with 420- and 430-nm interference filters) between two CCD cameras (MTI CCDC72, North Reading, MA). A Silicon Graphics workstation (St-Laurent, Quebec, Canada) captured identical 30-sec video sequences from both the 420- and 430-nm video tapes and stored the data on hard disk as two sets (one for each wavelength) of 900 image files in TIFF format.

Red blood cell (RBC) hemoglobin oxygen saturations (So_2) were computed for every second at every capillary segment location based on the 430-nm/420-nm optical density ratio, as previously described (22). The optical density of each flowing RBC was computed as OD = log (Io/I), where I is intensity of transmitted light passing through the RBC and Io is the intensity of incident light on the RBC. RBC oxygen saturation was computed as $So_2 = a + b \cdot OD430/OD420$, where constants a and b were determined from an *in vivo* calibration against 0 and 100% oxygen using a gas chamber inserted into the microscope stage.

Capillary geometry and RBC hemodynamics were determined from the 420-nm OD information. Flowing RBCs separated by plasma gaps generate varying OD information over time as they pass through the optical path. This variance in light intensity was used to generate a variance image, which outlined the geometry (length and diameter) of the flowing RBC column (high variance) against the tissue background (low variance) (21). Capillary RBC velocity (V; μm/sec) was computed using a frame-by-frame spatial correlation technique, and RBC lineal density (LD; RBC/mm) was determined by detecting the number of RBCs in a capillary segment in each video frame (20). The RBC supply rate (SR; RBC/sec) was calculated as the product of RBC velocity and lineal density, SR = V·LD (16).

Quantification of Capillary Oxygen Flow, Oxygen Extraction, and Oxygen Flux. Using RBC hemodynamic and oxygen saturation information, oxygen flow rates (qO_2) were calculated as the product of RBC supply rate and hemoglobin oxygen saturation, $qO_2 = SR \cdot So_2 \cdot K$, where K is the oxygen-carrying capacity of a single RBC ($K = 0.0362$ pL oxygen/RBC at 100% So_2) (16). Capillary oxygen extraction (O_2ER) was determined from oxygen flow rates at the entrance (en) and exit (ex) of a capillary segment, $O_2ER = (qO_2[en] - qO_2[ex])/qO_2(en)$. The rate of oxygen diffusion into the surrounding tissue per unit capillary surface area (flux of oxygen per $min^{-1} \mu m^{-2}$), or capillary oxygen flux (O_2flux), was calculated from oxygen flow rates and capillary geometry, $O_2flux = (qO_2[en] - qO_2[ex])/(\pi dL)$ (1), where πdL is the capillary surface area (d, diameter; L, length). Figure 1 outlines the geometry and mathematical equations used to calculate capillary oxygen flux, and Figure 2 provides an example of the O_2flux profile obtained from a single capillary over the 30-sec sampling period.

Indices for Tissue Oxygen Consumption and Oxygen Supply. Direct measurement of oxygen consumption in the tissue surrounding the capillaries was not possible; however, a tissue oxygen consumption index (CDper·O_2flux) could be calculated from the product of perfused capillary density (CDper) and capillary oxygen flux (O_2flux). The same rationale was applied to calculate a tissue oxygen supply index (CDper·qO_2[en]) from the product of perfused capillary density (CDper) and capillary oxygen flow rate (qO_2[en]).

Functional Capillary Density. While RBC hemodynamic and So_2 data were determined in single in-focus flowing capillaries, the field of view contained additional information on neighboring capillary flow behavior. To quantify this behavior, three horizontal reference lines perpendicular to muscle fibers (149 μm) were drawn on a transparent film and placed over the monitor (15, 19). During video playback, capillaries that intersected reference lines were evaluated over 30 secs. Flow behavior was categorized as continuous (cont), intermittent (int), or stopped (stop) and expressed as capillary density (CD; caps/mm). Total capillary density (CDtotal) is the sum of CDcont, CDint, and CDstop, while perfused capillary density (CDper) is the sum of CDcont and CDint.

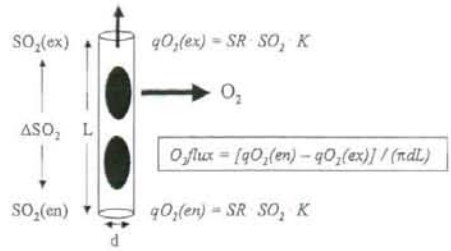

Figure 1. Schematic of O_2flux calculation. Red blood cells (RBC) flow in a capillary from bottom to top. As oxygen is off-loaded to the tissue, a red cell hemoglobin oxygen saturation gradient (ΔSO_2) develops across the length (L) of the capillary. From capillary geometry, red cell supply rate (where supply rate is the product of RBC velocity and lineal density [$SR = V \cdot LD$]), oxygen saturation (SO_2), and oxygen flow rates at the capillary segment entrance ($qO_2(en)$) and exit ($qO_2(en)$), a capillary oxygen flux (O_2flux is the rate of oxygen diffusing from capillary to tissue) can be calculated. πDL, surface area of the capillary; D, capillary diameter; K, oxygen-carrying capacity of the red blood cell.

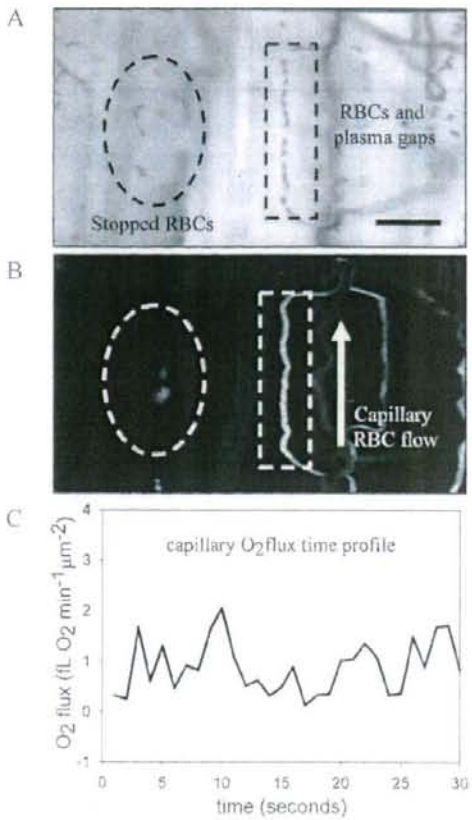

Figure 2. Example of capillary oxygen flux (O_2flux) profile. *A*, ×20 video frame of the rat hind limb extensor digitorum longus skeletal muscle microcirculation near the surface of the muscle. Dark objects are individual red blood cells (*RBCs*). *B*, 30-sec variance image depicting capillary flow (white lines against dark background). Note the capillary stopped-flow in the circled area. *C*, 30-sec O_2flux profile for the outlined capillary in *A*. Scale bar is 50 µm.

Arterial and Tissue NO_x^- Measurement. NO_x^- ($NO_2^- + NO_3^-$) was determined, as previously described (23). In brief, NO gas generated by chemical reduction of NO_x^- (0.05 M V(III) in 1 M HCl at 90°C) was detected by chemiluminescent reaction with ozone using an NO analyzer (Sievers 270b, Boulder, CO). The system was calibrated against known concentrations of NO_3^-. Arterial blood (250 µL) was collected isovolemically and deproteinized (1:1 whole blood/acetonitrile) to prevent hemoglobin interference (24). Samples were stored at −20°C and analyzed within 6 hrs. Frozen EDL tissue was homogenized in cold phosphate-buffered saline (1:15 wt/vol), filtered for 80 mins to remove tissue debris, and stored at −80°C before analysis.

Drug Dose and Delivery. To completely inhibit iNOS/NO overproduction, the specific iNOS inhibitor L-NIL (25–27) (Sigma, St. Louis, MO) was administered by venous infusion (3 mg·kg^{-1}·hr^{-1}) starting 1 hr after CLP.

Immunoblots for NOS Isoforms. To determine which NOS isoforms were up-regulated, Western blots were performed using a standard protocol as previously described (28). Briefly, frozen samples of EDL muscles were homogenized in five volumes (wt/vol) of homogenizing buffer (20 mM Tris-Cl, 1 mM EGTA, 1 mM EDTA, 1 mM DTT, 1 mM PMSF, 20 µg/mL leupeptin, and 1% triton × 100) and centrifuged (10,000 rpm for 20 mins at 4°C). The supernatant was mixed 1:1 with a sodium dodecyl sulfate glycerol buffer (125 mM Tris-HCl [pH 6.8], 20% glycerol, 4% sodium dodecyl sulfate, 2% β-mercaptoethanol, and 0.01% bromophenol blue), denatured at 95°C for 5–10 mins, resolved (25 µL/well) on a 7.5% polyacrylamide gel, and transferred to a polyvinylidene difluoride membrane. Membranes were blocked with 5% nonfat skim milk; incubated with mouse anti-neuronal NOS (nNOS) monoclonal antibody (mAb) (1:1000 in blocking buffer; BD Biosciences Transduction Laboratories, Mississauga, ON), mouse anti-endothelial NOS (eNOS) mAb (1:1000; BD Biosciences Transduction Laboratories), rabbit anti-iNOS polyclonal antibody (1:500; BD Biosciences Transduction Laboratories), or mouse anti-glyceraldehyde phosphate dehydrogenase mAb (1:10,000; Helena Biosciences, Hornby, ON) for 2 hrs; washed; and further incubated with the appropriate peroxidase-labeled anti-mouse or anti-rabbit immunoglobulin G antibody (1:1000, 1 hr at room temperature). Blots were washed and banding was visualized using an enhanced chemiluminescence kit (LUMIGLO, KPL laboratories, Gaithersburg, MA) with Kodak BIOMAX MR imaging film (Rochester, NY). Glyceraldehyde phosphate dehydrogenase was visualized using metal-enhanced DAB reagent (3,3'-diaminobenzidine; Roche Diagnostics, Laval, Quebec).

Statistical Analysis. Data are reported as median and range (25th–75th percentiles). Between-group differences in functional capillary density, oxygen transport, tissue NO_x^-, and blood gases were evaluated using non-

parametric Kruskal-Wallis one-way analysis of variance on ranks with multiple pairwise comparisons using Dunn's test. Within-group differences in blood NO_x^- and MAP over time were evaluated using nonparametric Friedman's one-way repeated measures analysis of variance on ranks with multiple pairwise comparisons against baseline using Dunnett's test. We considered $p < .05$ to be statistically significant. All statistical tests were performed using Systat, version 3.0 (Point Richmond, CA).

RESULTS

CLP Increases EDL Tissue and Blood NO_x^- Levels. Five hours after septic injury, iNOS protein expression increased in EDL skeletal muscle. There were no changes in either eNOS or nNOS protein expression (Fig. 3*A*). Corresponding with increased iNOS expression was a 68% increase ($p < .05$) in EDL tissue NO_x^- and a two-fold increase ($p < .05$) in arterial blood NO_x^- (Fig. 3, *B* and *C*, respectively). We pharmacologically targeted iNOS by constant infusion of the iNOS inhibitor L-NIL and found that both systemic NO_x^- and EDL tissue NO_x^- levels were maintained at baseline (Fig. 3, *B* and *C*). L-NIL treatment attenuated the fall in MAP observed in CLP animals but did not restore MAP to baseline (Fig. 3*D*). All animals survived 5 hrs after septic injury.

Sepsis Increases Capillary Stopped-Flow, and Inhibiting NO Overproduction in CLP Animals Increases EDL Capillary RBC Velocity. Visual assessment of capillary flow behavior in EDL skeletal muscle microvascular beds revealed that septic injury increased capillary stopped-flow 2.6-fold: CDstop was 7.7 (5.9–11.1) caps/mm in CLP vs. 2.3 (2.2–4.5) caps/mm in sham, respectively ($p < .05$, Table 1). Inhibiting iNOS/NO overproduction had no effect on capillary stopped-flow. Microvascular imaging analysis of continuous-flow capillaries revealed that RBC velocity was unchanged in CLP animals compared with sham but increased 48% when NO was inhibited in CLP animals: 105 (90.6–120) μm/sec in CLP vs. 148 (140–185) μm/sec in CLP+L-NIL ($p < .05$, Table 2). While RBC LD remained unchanged, the increase in RBC velocity resulted in a trend ($p = .12$) toward an increase in capillary RBC supply rate (SR = V·LD) in CLP+L-NIL animals. There were no differences in capillary geometry between groups.

Sepsis Increases the Capillary So_2 Gradient and Oxygen Flux, and Inhibiting NO Overproduction Increases Tissue Oxygen Consumption. Microvascular imaging analysis of RBC hemoglobin oxygen saturation (So_2) in continuous-flow capillaries revealed that sepsis increased So_2 gradients (ΔSo_2) along capillary segments in septic and iNOS/NO-inhibited septic animals (ΔSo_2 was 5.7% ± 2.0% in sham vs. 13.6% ± 4.6% in CLP and 15.8% ± 4.0% in CLP+L-NIL, $p < .05$, respectively, Table 2). We found oxygen flux (O_2flux) into the tissue increased in both CLP and CLP+L-NIL animals: O_2flux was 0.33 (0.26–0.72) fL oxygen $min^{-1}\mu m^{-2}$ in sham vs. 1.4 (1.2–1.6) fL oxygen $min^{-1}\mu m^{-2}$ in CLP and 1.5 (1.1–1.8) fL oxygen $min^{-1}\mu m^{-2}$ in CLP+LNIL, $p < .05$, respectively (Table 2).

By taking perfused capillary density into account, we were able to calculate indices for both local capillary oxygen delivery (CDper·qO_2[en]) and local tissue oxygen consumption (CDper·O_2flux). While there

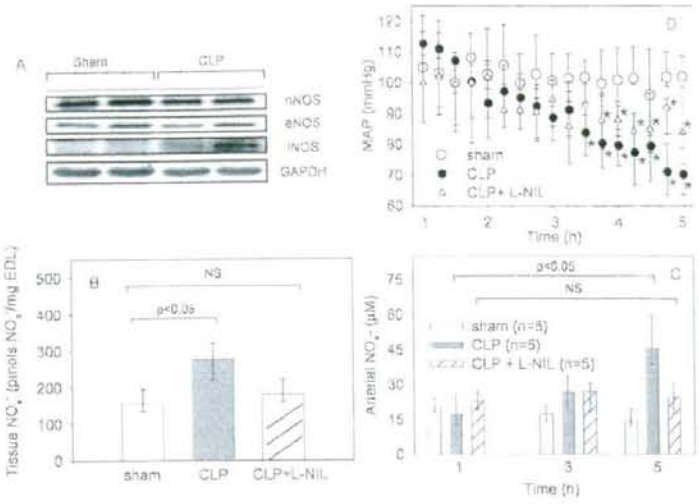

Figure 3. Sepsis-induced changes in extensor digitorum longus nitric oxide synthase (*NOS*) expression, tissue and blood NO_x^-, and mean arterial pressure (*MAP*). *A*, Western blot revealed that only inducible NOS (*iNOS*) protein expression increased by 5 hrs. Values are median and range (25th–75th percentiles). *B*, at 5 hrs, skeletal muscle tissue NO_x^- (NO_2^- + NO_3^-) was elevated, but inhibiting iNOS/NO maintained it at sham levels. *C*, similarly, arterial blood NO_x^- increased in cecal ligation and perforation (*CLP*) animals following septic injury and was maintained at baseline by treatment with L-N6-(1-iminoethyl)lysine dihydrochloride (*L-NIL*). *D*, MAP decreased following CLP, and inhibiting NO overproduction (*CLP+L-NIL*) partially restored MAP to baseline. Between-group differences in tissue NO_x^- level and within-group differences in blood NO_x^- and MAP over time were evaluated using Kruskal-Wallis one-way analysis of variance on ranks and Friedman's one-way repeated measures analysis of variance on ranks, respectively. *$p < .05$ vs. baseline. *nNOS*, neuronal NOS; *eNOS*, endothelial NOS; *GAPDH*, glyceraldehyde phosphate dehydrogenase; *NS*, not significant.

Table 1. Sepsis alters capillary flow behavior

	Sham	CLP	CLP + L-NIL	*p* Value
CDcont, caps/mm	16.2 (14.2–21.3)	16.8 (15.5–17.8)	19.1 (17.8–31.3)	NS
CDint, caps/mm	2.3 (0–3.1)	2.2 (1.3–7.5)	1.3 (0–2.9)	NS
CDstop, caps/mm	2.3 (2.2–4.5)	7.7 (6.0–11.1)[a]	9.5 (8.1–11.8)[a]	<.05
CDper, caps/mm	23.8 (20.6–26.3)	24.0 (17.2–24.2)	24.0 (19.7–32.9)	NS
ICD, Mm	43.7 (38.0–49.2)	41.6 (41.3–58.2)	41.6 (30.7–51.1)	NS
CDtotal, caps/mm	28.1 (25.0–29.0)	29.3 (28.0–31.5)	36.2 (30.7–38.8)	NS

CLP, cecal ligation and perforation; L-NIL, L-N6-(1-iminoethyl)lysine dihydrochloride; CDcont, continuous capillary density; NS, not significant; CDint, intermittent capillary density; CDstop, stopped capillary density; CDper, perfused flow capillary density; ICD, intercapillary distance; CDtotal, total V.

[a]$p < .05$ vs. sham. Capillary density was based on capillaries containing red blood cells. Capillary flow behavior was categorized over a 30-sec interval. CDper = CDcont + CDint, while CDtotal = CDcont + CDint + CDstop. Between-group differences were evaluated by Kruskal-Wallis one-way analysis of variance on ranks. Values are median and range (25th–75th percentiles).

Table 2. Capillary geometry, red blood cell (RBC) hemodynamics, and oxygen transport variables during septic shock

	Sham (n = 56)	CLP (n = 47)	CLP+LNIL (n = 43)	p Value
Geometry				
Length, μm	117 (103–118)	99 (95.6–121)	123 (113–126)	NS
Diameter, μm	5.5 (5.4–5.7)	5.6 (5.4–5.7)	5.4 (5.3–5.5)	NS
Hemodynamics				
Velocity, μm/sec	113 (109–139)	105 (90.7–120)	148 (140–185)[a]	<.05
Lineal density, RBC/mm	82.6 (70.4–104)	91.4 (85.6–104)	94.3 (75.2–106)	NS
Supply rate, RBC/sec	8.5 (5.9–9.1)	7.8 (6.8–8.2)	10.4 (8.1–16.1)	NS
Oxygen transport				
So_2(en), %	39.1 (32.2–43.4)	33.4 (30.4–46.2)	29.8 (29.0–48.1)	NS
So_2(ex), %	31.6 (29.2–33.2)	20.0 (14.9–28.8)	13.9 (11.4–21.6)[b]	<.05
ΔSo_2, %	6.3 (3.6–7.2)	14.5 (10.8–16.3)[b]	17.1 (13.1–18.1)[b]	<.05
qO_2(en), fL O_2 sec^{-1}	121 (111–169)	104 (101–198)	201 (119–226)	NS
qO_2(ex), fL O_2 sec^{-1}	109 (91.2–143)	89.6 (38.9–110)	91.9 (61.5–107)	NS
O_2ER, %	14.6 (12.9–17.0)	35.6 (29.4–41.9)	54.6 (45.5–62.9)[b]	<.05
O_2flux, fL O_2 min^{-1} μm^{-2}	0.33 (0.26–0.73)	1.4 (1.2–1.7)[b]	1.5 (1.1–1.8)[b]	<.05
CDper-qO_2(en), caps mm^{-1}· pL O_2 sec^{-1}	2.8 (1.8–4.2)	1.8 (1.8–2.0)	1.8 (1.7–2.9)	NS
CDper-O_2flux, caps mm^{-1}· fL O_2 min^{-1} μm^{-2}	4.2 (3.3–20.5)	22.5 (19.1–33.6)	45.2 (30.3–46.5)[b]	<.05

n, total number of capillaries analyzed in each group; CLP, cecal ligation and perforation; L-NIL, L-N6-(1-iminoethyl)lysine dihydrochloride; NS, not significant; So_2, oxygen saturation; en, entrance of capillary segment; ex, exit of capillary segment; ΔSo_2, RBC hemoglobin oxygen saturation gradient along a capillary segment; qO_2, oxygen flow rate; O_2ER, capillary oxygen extraction ratio; O_2flux, capillary oxygen flux; CDper, perfused capillary density.

[a]$p < .05$ vs. CLP; [b]$p < .05$ vs. sham. Values are median and range (25th–75th percentiles). Capillary length and diameter were determined from variance images (Figure 2*B*) and used to calculate capillary surface area. RBC hemodynamics and So_2 were used to calculate qO_2, O_2ER, and O_2flux. Indexes of local capillary oxygen delivery and local tissue oxygen consumption were approximated by CDper-qO_2(en) and CDper-O_2flux, respectively. Between-group differences were evaluated by Kruskal-Wallis one-way analysis of variance on ranks.

Table 3. Arterial blood gases at 5 hrs

	Sham	CLP	CLP+L-NIL	p Value
Pao_2, torr	92.6 (88.6–111)	109.4 (106–113)	98.6 (95.7–109)	NS
Sao_2, %	93.8 (90.0–98.4)	93.7 (92.1–95.5)	95.2 (93.5–96.6)	NS
$Paco_2$, torr	38.4 (37.2–40.0)	35.5 (33.7–37.0)	34.7 (33.0–35.9)	NS
pH	7.44 (7.42–7.45)	7.31 (7.30–7.37)[a]	7.40 (7.38–7.42)	<.05
Hb, g/dL	12.0 (11.3–12.2)	15.3 (15.1–15.9)[a]	14.3 (13.8–14.3)	<.05

CLP, cecal ligation and perforation; L-NIL, L-N6-(1-iminoethyl)lysine dihydrochloride; NS, not significant; Sao_2, arterial oxygen saturation; Hb, hemoglobin.

[a]$p < .05$ vs. sham. Normal Hb range in rat is 11.5–16 g/dL. Between-group differences were evaluated using Kruskal-Wallis one-way analysis of variance on ranks. Values are median and range (25th–75th percentiles).

was no detectable change in CDper-qO_2(en) between groups, there was a significant increase in CDper-O_2flux when nitric oxide overproduction was inhibited in septic animals ($p < .05$, Table 2), indicating that local EDL tissue oxygen consumption had increased when iNOS/NO overproduction was inhibited. This difference in oxygen consumption was reflected in changes in capillary oxygen extraction, where inhibiting iNOS/NO overproduction increased capillary oxygen extraction 43% above that of septic animals: from 35.5% (29.4–41.9) in CLP to 54.6% (45.5–62.9) in CLP+L-NIL, vs. 14.6% (12.9–16.9) in sham ($p < .05$, Table 2).

Blood Gases. Arterial Po_2, Pco_2, and So_2 were normal in all three groups at 5 hrs (Table 3). Arterial pH decreased in CLP animals: from 7.44 (7.42–7.45) in sham to 7.31 (7.30–7.37) in CLP ($p < .05$, Table 3). Inhibiting iNOS/NO overproduction prevented the fall in pH in CLP+L-NIL animals. Whole blood hemoglobin levels were elevated in CLP animals but remained within the normal rat physiologic range. Inhibiting NO overproduction in CLP+L-NIL animals maintained hemoglobin at sham level.

DISCUSSION

The key finding of this study was that inhibiting iNOS/NO overproduction during the onset of hypotensive sepsis increased skeletal muscle tissue oxygen consumption. We estimate that NO overproduction was able to reduce local EDL skeletal muscle oxygen consumption approximately 50%. This finding is in agreement with *in vitro* studies showing that NO donors inhibit mitochondrial respiration and reduce tissue oxygen consumption (3–5). Moreover, iNOS/NO overproduction modulates local *in vivo* oxygen consumption at a time when microvascular dysfunction and increased capillary stopped-flow lead to maldistribution of capillary red cell flow and increased heterogeneity of oxygen delivery. It is unknown what effect such a drop in mitochondrial respiration has on metabolic flux, energetic status, or cellular function, and this requires further investigation. However, evidence of increased capillary oxygen extraction and elevated arterial pH in iNOS/NO-inhibited septic animals is consistent with a shift toward increased aerobic metabolism. Early goal-directed therapy in septic patients, which attempted to balance oxygen delivery with oxygen demand, resulted in a similar increase in arterial pH (29).

Our animal study demonstrates that NO-mediated decrease in local skeletal muscle oxygen consumption occurs early in sepsis and can be prevented by maintaining NO production at baseline. Since Torres et al. (5) showed that NO competitively inhibits mitochondrial complex IV at low oxygen concentrations, one implication from our study is that increased oxygen demand and microvascular dysfunction establish microenvironmental Po_2 conditions that allow increased NO levels to outcompete reduced oxygen levels for binding to cytochrome *c* oxidase (complex IV), thereby reducing tissue oxygen consumption. While our study shows that the EDL tissue continues to consume oxygen and supports findings indicating that mitochondrial inhibition is reversible (2, 3), evidence of increased tissue Po_2, reduced complex I activity, and decreased adenosine triphosphate in skeletal muscle of septic patients (30, 31) suggests there is a transition at some point in the progression of sepsis from reversible to nonreversible mitochondrial

inhibition, allowing oxygen levels to increase in the tissue.

While much is known about the inflammatory and coagulation response to bacterial infection and trauma, the precise etiology of sepsis-induced multiorgan failure remains to be fully elucidated (32). In septic patients, changes in both sublingual microvascular perfusion density (33–35) and skeletal muscle mitochondrial electron transport activity (31) have been associated with sepsis severity and patient outcome. These findings implicate both microvascular dysfunction (local oxygen delivery and distribution) and mitochondrial respiration (local oxygen consumption) as critical factors in sepsis. In our animal study, we provide evidence that both local microvascular oxygen distribution and local oxygen consumption are altered during the onset of septic injury, suggesting that both factors are involved concurrently in modulating tissue metabolism and possibly muscle function. If similar microvascular dysfunction and local tissue hypoxia occurred in other organs including the liver, kidney, and heart (36, 37) at a time when iNOS was up-regulated and NO overproduced, it is possible that NO-mediated decreased mitochondrial function and reduced local oxygen consumption could contribute to alterations in organ function.

Microvascular Function, Oxygen Transport, and Nitric Oxide. Inhibiting iNOS/NO overproduction had the concurrent effects of increasing local tissue oxygen consumption while increasing capillary RBC velocity. It failed, however, to prevent capillary stopped-flow. Our finding of increased local RBC velocity was supported by Gocan et al. (38), who found that inhibiting nNOS in rat septic skeletal muscle at 24 hrs restored arteriolar responsiveness to acetylcholine and increased downstream capillary RBC velocity. It is not clear, however, how inhibiting iNOS at 5 hrs and nNOS at 24 hrs produces similar microvascular effects. The discrepancy may be related to a shift in NOS profile over time (38, 39) as both nNOS and iNOS affect arteriolar function during sepsis (28, 40). The failure of L-NIL to prevent capillary stopped-flow, however, was in contrast to our findings with the widely used iNOS inhibitor aminoguanidine, which attenuated increased stopped-flow (15). We suspect this discrepancy is because aminoguanidine has both NOS inhibition and antioxidant properties (41), whereas L-NIL does not. While reports show that NO controls capillary perfusion during hypoxia in normal animals (42) and oxidative stress (43) affects capillary density during sepsis, further research is required to fully elucidate the cause and effect relationships between NO and reactive oxygen species on capillary perfusion under pathologic conditions.

Clinical Relevance. The concept of NO inhibition as a therapy for sepsis is still debatable. Despite discontinuation of a clinical trial assessing the nonspecific NOS inhibitor 546C88 (12), this unexpected result was in contrast to the trend toward reduced mortality observed in its phase II clinical study. Thus significant differences existed between the methodologies of these two trials that resulted in a greater number of patients receiving the high dose of nonspecific NOS inhibitor in the prematurely discontinued multicenter trial. Our results in an animal model suggest that early inhibition of iNOS/NO overproduction and maintenance of NO levels at baseline could be potentially beneficial (i.e., increased local oxygen consumption in skeletal muscle) despite incomplete restoration of MAP to baseline. Increasing the dose of iNOS inhibitor to fully restore MAP may impose a detrimental effect, by increasing systemic vascular resistance and reducing cardiac output and oxygen delivery to tissues already stressed by a dysfunctional microcirculation. This raises important clinical questions: Can targeted NOS inhibition be beneficial if started early enough? To what degree should NO be inhibited to achieve a beneficial effect? The primary cause of death in the randomized trial was cardiac decompensation; however, it is unclear to what degree NO was inhibited. Further research is required to determine whether there is a window for a beneficial effect of inhibiting NO overproduction during sepsis.

Study Limitations. We obtained capillary oxygen transport and tissue oxygen consumption information at the local capillary/tissue interface and not over the entire tissue. The imaging system is limited to capillaries with RBC velocities <1000 μm/sec and lineal densities of 180 RBC/mm, which precludes measurement of a smaller number of capillaries, perhaps 10% to 15% (19) with hyperflow. Biosimulations indicate that these vessels supply large amounts of oxygen to the tissue (17); however, we were unable to assess oxygen consumption in these local areas. A second limitation was our focus on iNOS/NO exclusively. Reports indicate that eNOS is capable of regulating mitochondrial respiration under normal conditions (7, 44), although we suspect its influence to be minimal under septic conditions as iNOS is the source of NO overproduction. The possibility that neuronal NOS or its splice variant, the putative mitochondrial NOS (45), inhibits mitochondrial respiration in sepsis is intriguing and warrants further investigation. An additional study limitation is that while we found no evidence of increased MAP following L-NIL infusion, suggesting that L-NIL did not nonspecifically inhibit eNOS, treating sham animals with L-NIL may have uncovered any nonspecific NOS inhibition effects.

CONCLUSION

During the onset of hypotensive sepsis, iNOS/NO overproduction reduces tissue oxygen consumption in rat skeletal muscle. Concurrent microvascular dysfunction may facilitate this phenomenon by reducing the Po_2 in the tissue microenvironment.

ACKNOWLEDGMENTS

We acknowledge the technical assistance of Stephanie Milkovich with calibration of the spectrophotometric functional imaging, and we thank Karey Shumansky for reviewing the statistical analyses.

REFERENCES

1. Bateman RM, Sharpe MD, Ellis CG: Bench-to-bedside review: Microvascular dysfunction in sepsis—hemodynamics, oxygen transport, and nitric oxide. *Crit Care* 2003; 7:359–373
2. Davies NA, Cooper CE, Stidwill R, et al: Inhibition of mitochondrial respiration during early stage sepsis. *Adv Exp Med Biol* 2003; 530:725–736
3. Clementi E, Brown GC, Feelisch M, et al: Persistent inhibition of cell respiration by nitric oxide: Crucial role of S-nitrosylation of mitochondrial complex I and protective action of glutathione. *Proc Natl Acad Sci U S A* 1998; 95:7631–7636
4. Frost MT, Wang Q, Moncada S, et al: Hypoxia accelerates nitric oxide-dependent inhibition of mitochondrial complex I in activated macrophages. *Am J Physiol Regul Integr Comp Physiol* 2005; 288:R394–R400
5. Torres J, Darley-Usmar V, Wilson MT: Inhibition of cytochrome c oxidase in turnover by nitric oxide: Mechanism and implications for control of respiration. *Biochem J* 1995; 312: 169–173
6. Anning PB, Sair M, Winlove CP, et al: Abnormal tissue oxygenation and cardiovascular

changes in endotoxemia. *Am J Respir Crit Care Med* 1999; 159:1710–1715
7. Shen W, Hintze TH, Wolin MS: Nitric oxide: An important signaling mechanism between vascular endothelium and parenchymal cells in the regulation of oxygen consumption. *Circulation* 1995; 92:3505–3512
8. Siegemund M, van Bommel J, Schwarte LA, et al: Inducible nitric oxide synthase inhibition improves intestinal microcirculatory oxygenation and CO2 balance during endotoxemia in pigs. *Intensive Care Med* 2005; 31: 985–992
9. Avontuur JA, Tutein Nolthenius RP, van Bodegom JW, et al: Prolonged inhibition of nitric oxide synthesis in severe septic shock: A clinical study. *Crit Care Med* 1998; 26: 660–667
10. Broccard A, Hurni JM, Eckert P, et al: Tissue oxygenation and hemodynamic response to NO synthase inhibition in septic shock. *Shock* 2000; 14:35–40
11. Watson D, Grover R, Anzueto A, et al: Cardiovascular effects of the nitric oxide synthase inhibitor NG-methyl-L-arginine hydrochloride (546C88) in patients with septic shock: Results of a randomized, double-blind, placebo-controlled multicenter study (study no. 144-002). *Crit Care Med* 2004; 32:13–20
12. Lopez A, Lorente JA, Steingrub J, et al: Multiple-center, randomized, placebo-controlled, double-blind study of the nitric oxide synthase inhibitor 546C88: Effect on survival in patients with septic shock. *Crit Care Med* 2004; 32:21–30
13. Grover R, Zaccardelli D, Colice G, et al: An open-label dose escalation study of the nitric oxide synthase inhibitor, N(G)-methyl-L-arginine hydrochloride (546C88), in patients with septic shock. Glaxo Wellcome International Septic Shock Study Group. *Crit Care Med* 1999; 27:913–922
14. Statman R, Cheng W, Cunningham JN, et al: Nitric oxide inhibition in the treatment of the sepsis syndrome is detrimental to tissue oxygenation. *J Surg Res* 1994; 57:93–98
15. Bateman RM, Jagger JE, Sharpe MD, et al: Erythrocyte deformability is a nitric oxide-mediated factor in decreased capillary density during sepsis. *Am J Physiol Heart Circ Physiol* 2001; 280:H2848–2856
16. Ellis CG, Bateman RM, Sharpe MD, et al: Effect of a maldistribution of microvascular blood flow on capillary O(2) extraction in sepsis. *Am J Physiol Heart Circ Physiol* 2002; 282:H156–H164
17. Goldman D, Bateman RM, Ellis CG: Effect of sepsis on skeletal muscle oxygen consumption and tissue oxygenation: Interpreting capillary oxygen transport data using a mathematical model. *Am J Physiol Heart Circ Physiol* 2004; 287:H2535–H2544
18. Goldman D, Bateman RM, Ellis CG: Effect of decreased oxygen supply on skeletal muscle oxygenation and oxygen consumption during sepsis: Role of heterogeneous capillary spacing and blood flow. *Am J Physiol Heart Circ Physiol* 2006; 290:H2277–H2285
19. Lam C, Tyml K, Martin C, et al: Microvascular perfusion is impaired in a rat model of normotensive sepsis. *J Clin Invest* 1994; 94: 2077–2083
20. Japee SA, Pittman RN, Ellis CG: A new video image analysis system to study red blood cell dynamics and oxygenation in capillary networks. *Microcirculation* 2005; 12:489–506
21. Japee SA, Ellis CG, Pittman RN: Flow visualization tools for image analysis of capillary networks. *Microcirculation* 2004; 11:39–54
22. Ellsworth ML, Pittman RN, Ellis CG: Measurement of hemoglobin oxygen saturation in capillaries. *Am J Physiol* 1987; 252: H1031–H1040
23. Bateman RM, Ellis CG, Freeman DJ: Optimization of nitric oxide chemiluminescence operating conditions for measurement of plasma nitrite and nitrate. *Clin Chem* 2002; 48:570–573
24. Bateman RM, Ellis CG, Sharpe MD, et al: Effect of hemolyzed plasma on the batch measurement of nitrate by nitric oxide chemiluminescence. *Clin Chem* 2001; 47: 1847–1851
25. Chlopicki S, Olszanecki R, Jakubowski A, et al: L-N6-(1-iminoethyl)-lysine (L-NIL) but not S-methylisothiourea sulphate (SMT) displays selectivity towards NOS-2. *Pol J Pharmacol* 1999; 51:443–447
26. Hansel TT, Kharitonov SA, Donnelly LE, et al: A selective inhibitor of inducible nitric oxide synthase inhibits exhaled breath nitric oxide in healthy volunteers and asthmatics. *FASEB J* 2003; 17:1298–1300
27. Moore WM, Webber RK, Jerome GM, et al: L-N6-(1-iminoethyl)lysine: A selective inhibitor of inducible nitric oxide synthase. *J Med Chem* 1994; 37:3886–3888
28. McKinnon RL, Lidington D, Bolon M, et al: Reduced arteriolar conducted vasoconstriction in septic mouse cremaster muscle is mediated by nNOS-derived NO. *Cardiovasc Res* 2005; 69:236–244
29. Rivers E, Nguyen B, Havstad S, et al: Early goal-directed therapy in the treatment of severe sepsis and septic shock. *N Engl J Med* 2001; 345:1368–1377
30. Boekstegers P, Weidenhofer S, Kapsner T, et al: Skeletal muscle partial pressure of oxygen in patients with sepsis. *Crit Care Med* 1994; 22:640–650
31. Brealey D, Brand M, Hargreaves I, et al: Association between mitochondrial dysfunction and severity and outcome of septic shock. *Lancet* 2002; 360:219–223
32. Hotchkiss RS, Karl IE: The pathophysiology and treatment of sepsis. *N Engl J Med* 2003; 348:138–150
33. Sakr Y, Dubois MJ, De Backer D, et al: Persistent microcirculatory alterations are associated with organ failure and death in patients with septic shock. *Crit Care Med* 2004; 32:1825–1831
34. Trzeciak S, Dellinger RP, Parrillo JE, et al: Early microcirculatory perfusion derangements in patients with severe sepsis and septic shock: Relationship to hemodynamics, oxygen transport, and survival. *Ann Emerg Med* 2007; 49:88–98
35. De Backer D, Creteur J, Preiser JC, et al: Microvascular blood flow is altered in patients with sepsis. *Am J Respir Crit Care Med* 2002; 166:98–104
36. Bateman RM, Tokunaga C, Kareco T, et al: Myocardial hypoxia-inducible HIF-1α, VEGF, and GLUT1 gene expression is associated with microvascular and ICAM-1 heterogeneity during endotoxemia. *Am J Physiol Heart Circ Physiol* 2007; 293:H448–H456
37. Tokunaga C, Bateman RM, Boyd J, et al: Albumin resuscitation improves ventricular contractility and myocardial tissue oxygenation in rat endotoxemia. *Crit Care Med* 2007; 35:1341–1347
38. Gocan NC, Scott JA, Tyml K: Nitric oxide produced via neuronal NOS may impair vasodilatation in septic rat skeletal muscle. *Am J Physiol Heart Circ Physiol* 2000; 278: H1480–H1489
39. Scott JA, Mehta S, Duggan M, et al: Functional inhibition of constitutive nitric oxide synthase in a rat model of sepsis. *Am J Respir Crit Care Med* 2002; 165:1426–1432
40. Hollenberg SM, Broussard M, Osman J, et al: Increased microvascular reactivity and improved mortality in septic mice lacking inducible nitric oxide synthase. *Circ Res* 2000; 86:774–778
41. Yildiz G, Demiryurek AT, Sahin-Erdemli I, et al: Comparison of antioxidant activities of aminoguanidine, methylguanidine and guanidine by luminol-enhanced chemiluminescence. *Br J Pharmacol* 1998; 124:905–910
42. Bertuglia S, Giusti A: Role of nitric oxide in capillary perfusion and oxygen delivery regulation during systemic hypoxia. *Am J Physiol Heart Circ Physiol* 2005; 288:H525–H531
43. Tyml K, Li F, Wilson JX: Delayed ascorbate bolus protects against maldistribution of microvascular blood flow in septic rat skeletal muscle. *Crit Care Med* 2005; 33:1823–1828
44. Loke KE, McConnell PI, Tuzman JM, et al: Endogenous endothelial nitric oxide synthase-derived nitric oxide is a physiological regulator of myocardial oxygen consumption. *Circ Res* 1999; 84:840–845
45. Persichini T, Mazzone V, Polticelli F, et al: Mitochondrial type I nitric oxide synthase physically interacts with cytochrome c oxidase. *Neurosci Lett* 2005; 384:254–259

Research

Open Access

Fibrinogen decreases cardiomyocyte contractility through an ICAM-1-dependent mechanism

John H Boyd, Edmond H Chau, Chiho Tokunanga, Ryon M Bateman, Greg Haljan, Ehsan Y Davani, Yinjin Wang and Keith R Walley

University of British Columbia Critical Care Research Laboratories, St. Paul's Hospital, 1081 Burrard Street, Vancouver, BC, V6Z 1Y6, Canada

Corresponding author: John H Boyd, jboyd@mrl.ubc.ca

Received: 18 Jul 2007 Revisions requested: 5 Sep 2007 Revisions received: 14 Oct 2007 Accepted: 3 Jan 2008 Published: 3 Jan 2008

Critical Care 2008, 12:R2 (doi:10.1186/cc6213)
This article is online at: http://ccforum.com/content/12/1/R2

Abstract

Introduction Cardiomyocytes exposed to inflammatory processes express intracellular adhesion molecule-1 (ICAM-1). We investigated whether fibrinogen and fibrinogen degradation products, including D-dimer, could alter cardiomyocyte contractile function through interaction with ICAM-1 found on inflamed cardiomyocytes.

Methods *In vivo*, rats were injected with endotoxin to model systemic inflammation, whereas isolated rat cardiomyocytes were treated with tumor necrosis factor-alpha to model the inflammatory environment seen following exposure to bacterial products such as lipopolysaccharide.

Results *In vivo*, endotoxin administration profoundly decreased cardiac contractile function associated with a large increase in intracardiac ICAM-1 and perivascular fibrinogen. Confocal microscopy with double-staining of isolated rat cardiomyocytes demonstrated colocalization of ICAM-1 and fibrinogen. This interaction was disrupted through pre-treatment of the cells with an ICAM-1-blocking antibody. Functionally, isolated rat cardiomyocyte preparations exhibited decreased fractional shortening when incubated with fibrinogen, and through the use of synthetic peptides, we determined that residues 117–133 of the fibrinogen gamma chain are responsible for this interaction with ICAM-1. Despite having crosslinked gamma chains, D-dimer retained the ability to decrease cardiomyocyte contractility.

Conclusion Site 117–133 of the fibrinogen gamma chain is able to depress cardiomyocyte contractility through binding ICAM-1.

Introduction

Both local and systemic inflammation impair cardiac contractility, although the precise mechanism behind this is still unclear [1-3]. It is now recognized that high levels of inflammatory biomarkers such as C-reactive protein and D-dimer are associated with an increased incidence of, and worse prognosis for, cardiovascular disease [4-8]. However, whether these molecules are simply markers of the inflammatory process or might actually play a causative role in the resultant organ dysfunction is not known. We previously reported a novel two-step regulatory mechanism of cardiomyocyte contractility whereby systemic inflammation induces cardiomyocyte-expressed intracellular adhesion molecule-1 (ICAM-1), whose subsequent ligation results in decreased contractility by signaling via the cytoskeleton [9]. While studies using cardiomyocyte/leukocyte co-culturing methods demonstrate that activated leukocytes can bind to ICAM-1 with a resultant decrease in myocardial contractility [9-11], we and others have noted a paucity of intramyocardial leukocytes in whole animal models of inflammation [12,13]. Therefore, we postulated that in the more complex environment of an *in vivo* model, ICAM-1 ligands other than the CD11/CD18 receptors found on activated leukocytes [14-16] play a greater role in ICAM-1-dependent decreases in cardiomyocyte contractility.

Fibrinogen, a 340-kDa plasma glycoprotein with a physiological plasma concentration of 1.5 to 4.5 g/L, as well as its related protein fragments D-dimer and other fibrinogen degra-

BSA = bovine serum albumin; EDV = end diastolic volume; E_{es} = end-systolic elastance; EF = ejection fraction; ELISA = enzyme-linked immunosorbent assay; E_{max} = maximal end-systolic elastance; FDP = fibrinogen degradation product; FITC = fluorescein isothiocyanate; ICAM-1 = intracellular adhesion molecule-1; Ig = immunoglobulin; LAD = left anterior descending; LPS = lipopolysaccharide; PBS = phosphate-buffered saline; TNF-α = tumor necrosis factor-alpha; vWF = von Willebrand factor; XL = crosslinking.

dation products (FDPs) represent potential ICAM-1-binding myocardial depressant substances. The amino acid sequence 117–133 of fibrinogen gamma chain (fg-γ-117–133) binds to the amino acid sequence 8–22 (ICAM-1-8–22) within the first immunoglobulin (Ig) domain of ICAM-1 [17]. The functional role of the fibrinogen-ICAM-1 interaction includes adhesion of leukocytes to endothelial cells [18,19], leukocyte transmigration [20], and promotion of endothelial cell survival [21]. Interestingly, fibrinogen-ICAM-1 ligation leads to cytoskeleton-dependent ERK1/2 (extracellular signal-regulated kinase-1/2) phosphorylation in endothelial cells [22]. In view of our previous observation in cardiomyocytes that ICAM-1 ligation by leukocytes reduces contractility via focal adhesion kinase phosphorylation at the cytoskeleton [9], fibrinogen-ICAM-1 ligation ultimately could lead to alteration in cardiomyocyte contractile function. As fragments of polymerized fibrinogen such as D-dimer are markedly elevated in most inflammatory states [4-8], it is of particular interest to determine whether these molecules are able to influence cardiac physiology through interaction with ICAM-1.

The goal of our study, therefore, was to determine whether exposure to fibrinogen and FDPs altered the contractile function of cardiomyocytes. To simulate systemic inflammation, rats were injected with endotoxin, and through immunohistochemistry, we confirmed an increase in both cardiomyocyte-expressed ICAM-1 as well as increased intramyocardial fibrinogen deposition. In isolated cardiomyocytes exposed to an inflammatory environment, we established the specificity of the fibrinogen-ICAM-1 interaction and went on to determine the active site on fibrinogen responsible for ICAM-1-mediated alterations in contractility.

Materials and methods

This study was approved by the University of British Columbia Animal Care Committee and adheres to the Canadian and National Institutes of Health guidelines for animal experimentation.

In vivo experimental models

For the endotoxin model of inflammation, male Sprague-Dawley rats 350 to 450 g in weight were injected intraperitoneally with lipopolysaccharide (LPS) (10 mg/kg) or vehicle control (normal saline). The LPS dosage was selected as a midrange dosage of endotoxemic models that result in a hemodynamic effect [23,24]. The heart was excised 6 hours after injection, embedded in Optimal Cutting Temperature compound (Electron Microscopy Sciences, Hatfield, PA, USA), frozen in dry-ice-chilled isopentane, and stored at -80°C.

Measurement of left ventricular contractility and cardiac function

Left ventricular contractility and other measures of ventricular function were determined from pressure-volume measurements using Pressure-Volume Analysis software (PVAN 2.9; Millar Instruments Inc., Houston, TX, USA). Six to ten pressure-volume loops during a vena cava occlusion were sampled and used to measure end-systolic elastance (E_{es}), which is the slope of the end-systolic pressure-volume relationship relatively insensitive to changes in preload and afterload [25]. E_{max} is defined as the maximal E_{es}. The volume axis intercept, Vd, was considered zero volume for the steady-state measurements. Pressure-volume loops measured during steady-state conditions were used to measure the maximum rate of change of intraventricular pressure during isovolumic systole divided by end diastolic volume (EDV), $(dP/dt_{max})/EDV$, which is a sensitive isovolumic phase measure of left ventricular contractility [26], as well as to calculate ejection fraction (EF). End-systolic pressure during steady state was used as a measure of systemic arterial pressure afterload.

Immunofluorescent imaging with quantification

Frozen heart sections (6 μm) were acetone-fixed and incubated with universal blocking agent (DakoCytomation, Glostrup, Denmark). Fibrinogen and von Willebrand factor (vWF), a marker for the endothelium, were stained together to assess whether infiltration of fibrinogen into the myocardium occurred. Sections were incubated with 1:20 fluorescein isothiocyanate (FITC)-conjugated goat anti-mouse fibrinogen (Nordic Immunological Laboratories, Tilburg, The Netherlands) and 1:200 rabbit anti-mouse vWF (DakoCytomation) primary antibody and then labeled with Alexa Fluor 594 goat anti-rabbit antibody (Invitrogen Corporation, Carlsbad, CA, USA). Nuclei were stained with the Hoechst stain (Invitrogen Corporation). Control sections were incubated with FITC-conjugated non-specific goat IgG (Santa Cruz Biotechnology, Inc., Santa Cruz, CA, USA) and non-specific rabbit IgG (DakoCytomation) and processed in identical conditions.

Immunofluorescent ICAM-1 staining was carried out by incubating sections with 1:500 mouse anti-rat ICAM-1 monoclonal antibody 1A29 (BD Biosciences, San Jose, CA, USA) and then with Alexa Fluor 594-labeled goat anti-mouse antibody (Invitrogen Corporation). Control sections were incubated with non-specific mouse IgG (Invitrogen Corporation). After drying, the slides were mounted with DABCO (1,4-diazabicyclo[2.2.2]octane) to prevent photobleaching.

Images were captured using a laser scanning confocal microscope with a 63× water immersion lens (Leica SP2; Leica, Wetzler, Germany). Samples were imaged using fluorescence with wavelength excitations and emissions of 488 nm and 495 to 580 nm (respectively) for fibrinogen and 594 nm and 600 to 700 nm (respectively) for vWF and ICAM-1. The scan format was 512 × 512 pixels. Image capturing was performed sequentially using a three-frame average. All imaging was performed under identical microscope settings (for example, laser intensity and photomultiplier tube gain).

Cross-sections of 15 randomly selected blood vessels, identified via vWF staining, were imaged. Two ellipses were traced around each vessel: a small ellipse positioned closely along the vessel boundary and a large ellipse with proportional major and minor axes but three times the area of the small ellipse. Fibrinogen staining present in the annulus between the two ellipses was identified as perivascular fibrinogen. The sum fluorescence intensity per annulus area was measured using the Leica software.

To measure myocardial ICAM-1 expression, heart sections from the endotoxemic and control groups were imaged as described above and fluorescent intensity measures were taken using traced field areas containing myocardial tissue. The sum fluorescence intensity per unit area was measured using the Leica software.

Isolation of rat ventricular myocytes

Male Sprague-Dawley rats were injected with heparin and anesthetized using isofluorane. The heart was excised, mounted on a modified Langendorff apparatus, and digested with 281 U/mL collagenase (Worthington Biochemical Corporation, Lakewood, NJ, USA). After digestion, the cells were resuspended in modified Eagle's medium containing increasing Ca^{2+} concentrations (200 μM, 500 μM, and 1 mM). Five hundred thousand cells in M199 with bovine serum albumin (BSA) were loaded into a laminin-coated Petri dish 6 cm in diameter (BD Biosciences) and the cardiomyocytes were incubated for 12 hours to allow them to become relatively quiescent. After 24 hours, cells were considered viable if they demonstrated a characteristic rod shape without cytoplasmic blebbing.

Measurement of cardiomyocyte fractional shortening

Cells were paced at 1 Hz using a Grass S48 stimulator (Grass-Telefactor, Warwick, RI, USA) with a voltage set at 120% of the threshold capture voltage. Images were captured using a Myocam video camera (IonOptix Corporation, Milton, MA, USA) and analyzed using an IonOptix Softedge detection package (IonOptix Corporation). Fractional shortening was calculated as the difference between diastolic and systolic lengths, divided by diastolic length.

Coating of fibrinogen to polystyrene beads

Polystyrene beads 8 μm in diameter (Bangs Laboratories, Inc., Fishers, IN, USA) were washed twice with acetate buffer (pH 5.4). Beads were mixed with rat fibrinogen (Enzyme Research Laboratories, South Bend, IN, USA) at a concentration of 300,000 beads per microgram of fibrinogen in a 500-μL Eppendorf tube. A micromagnetic stir bar was placed in the tube, and the mixture was gently stirred for 2 hours at room temperature. The beads were then washed three times with fresh acetate buffer. Clumps of fibrinogen-coated beads were broken apart by passing them through a syringe with a 27.5-guage needle.

ICAM-1 peptide-fibrinogen binding assay

Ninety-six-well Corning Costar 9018 enzyme-linked immunosorbent assay (ELISA) plates (eBioscience, Inc., San Diego, CA, USA) were coated for 2 hours at room temperature with fibrinogen concentrations ranging from 0.01 to 100 nM in bicarbonate/carbonate coating buffer (3.03 g of Na_2CO_3, 6.0 g of $NaHCO_3$ per 1,000 mL of distilled water) (pH 9.6). Wells were washed with phosphate-buffered saline (PBS) and then blocked overnight with 1% BSA. One hundred micromolar biotinylated ICAM-1 (8–22) sequence EAFLPRGGSVQVNCS or biotinylated scrambled peptide sequence SCNVQVSGGRPLFAE (University of British Columbia Peptide Facility, Vancouver, BC, Canada) was then added to the wells and incubated for 2 hours at room temperature before washing three times with PBS. HRP-linked anti-biotin antibody (1 μg/mL) (Invitrogen Corporation) was then added and incubated for 2 hours, followed by three washes. One hundred microliters of ABTS (2,2'-azino-di(3-ethylbenzthiazoline sulfonate) solution (Chemicon International, Temecula, CA, USA) was added to each well and incubated for 60 minutes. Absorbance values were measured at 405 nm and at 492 nm for reference.

Incubations

Twenty-four hours after cardiomyocyte isolation, cells were activated with tumor necrosis factor-alpha (TNF-α) (20 ng/mL) for 4 hours to upregulate ICAM-1 expression [9]. In studies using fibrinogen-coated beads, 25,000 beads were added to cells in laminin-coated 96-well plates (500 cells per well). A bead that moved with the contracting cardiomyocyte and maintained a contact relative location on the membrane during contraction was considered to be adherent. In studies using rat fibrinogen (Enzyme Research Laboratories), human fibrinogen, D-dimer fragments D and E (HYPHEN BioMed, Neuville-sur-Oise, France), and fibrinogen gamma chain (AnaSpec, Inc., San Jose, CA, USA) cells were incubated at concentrations of 0.03 μM, 0.1 μM, 0.3 μM, and 1 μM, respectively, for 4 hours at 37°C. After 4 hours at 37°C, cardiomyocyte fractional shortening was measured as described above.

In studies using the ICAM-1 (8–22) sequence EAFLPRGGSVQVNCS or scrambled peptide sequence SCNVQVSGGRPLFAE (University of British Columbia Peptide Facility), 1 μM rat fibrinogen and 100 μM ICAM-1 (8–22) or scrambled peptide were mixed and incubated for 4 hours at 37°C prior to incubation with cardiomyocytes as described above. In studies using anti-ICAM-1-blocking monoclonal antibody 1A29 (BD Biosciences), the antibody was added to cardiomyocytes at a concentration of 200 ng/mL 4 hours prior to the addition of fibrinogen.

Colocalization of ICAM-1 with fibrinogen

Upon TNF-α activation, cardiomyocytes were co-cultured with Oregon Green-labeled fibrinogen (Invitrogen Corporation) for 4 hours. They were then fixed with 3% paraformaldehyde for